Julia Schmid

Gamma Ray Bursts with Antares

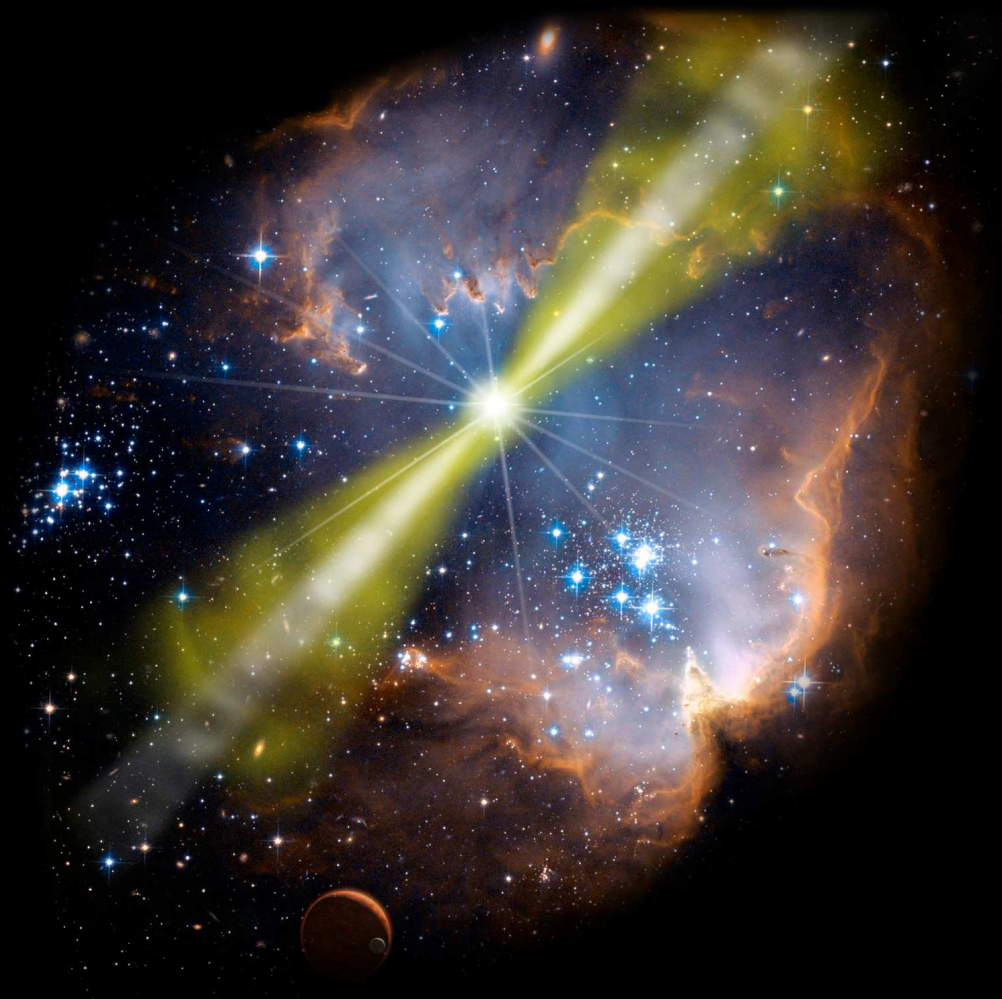

ECAP-2011-001

Physikalisches Institut der Universität Erlangen-Nürnberg

Diplomarbeit

Gamma Ray Bursts with Antares

Julia Schmid

beutreut durch

Prof. Dr. Gisela Anton

Erlangen, den 26.01.2011

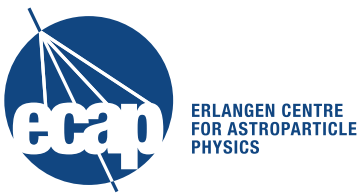

Image on frontpage: An artist's impression of a Gamma Ray Burst, picture courtesy *NASA/Swift*/Mary Pat Hrybyk-Keith and John Jones.

ZUSAMMENFASSUNG

Diese Arbeit untersucht, wie eine Gamma Ray Burst Analyse mit dem ANTARES Neutrino Teleskop durchgeführt werden könnte. Gamma Ray Bursts sind kurze, sehr intensive Blitze hochenergetischer Gammastrahlung, die unvorhersagbar und gleichmäßig verteilt am Himmel vorkommen. Innerhalb weniger Sekunden wird in diesen Explosionen so viel Energie ausgestrahlt, wie der Sonne während ihrer gesamten Lebenszeit zur Verfügung steht. Viele dieser Gammastrahlen–Ausbrüche werden mittlerweile mit einer bestimmten Art von Supernovae in Verbindung gebracht, in deren evolutionären Endstadium man die Bildung eines Schwarzen Loches vermutet.

Die Emission der elektromagnetischen Strahlung wird gemeinhin durch kollimierte hochrelativistische Ausbrüche von Materie erklärt, in denen sich Schockfronten bilden können. Darin werden Elektronen beschleunigt, was zur Abstrahlung hochenergetischer Gamma–Photonen führt. Man nimmt an, dass sich in den Schocks jedoch außerdem baryonische Materie befindet, die zusammen mit den Elektronen beschleunigt wird. Dies wäre eine mögliche Erklärung für die höchstenergetische Kosmische Strahlung, deren Ursprung bis heute ungeklärt ist. Falls diese Annahme gerechtfertigt ist, so erwartet man von hochrelativistischen Protonen die Aussendung von Neutrinos, die das elektromagnetische Signal des GRBs begleiten.

In dieser Arbeit wird eine Strategie zur Detektion eines GRB Neutrino Signals mit dem ANTARES–Experiment anhand von Monte–Carlo Simulationen untersucht. Die Vorgehensweise ist grundsätzlich auf alle Bursts anwendbar, wird aber exemplarisch am Beispiel des Bursts GRB080218B durchgeführt. Die Monte–Carlo Daten wurden dergestalt angepasst, dass sie den Neutrino–Fluss des Bursts und die Bedingungen des ANTARES Detektors zur entsprechenden Zeit simulieren. Zudem wurde echter optischer Untergrund, der zu dieser Zeit aufgenommen wurde, hinzugefügt, um eine möglichst realistische Studie zu erlauben. Die Analyse dieser Daten wurde dahingehend optimiert, dass sie bei Anwendung auf echte Daten eine statistisch möglichst signifikante Entdeckung liefert.

Außerdem wird eine Methode analysiert, mit der man möglicherweise systematische Fehler der Winkelrekonstruktion korrigieren und dadurch ihre Winkelauflösung verbessern könnte. Dafür wird zunächst anhand von Monte–Carlo Simulationen einiger Teilchenspuren im Detektor untersucht, ob grundsätzlich eine solche systematische Verschiebung vorliegt. Es konnte gezeigt werden, dass für einige dieser Spuren durchaus eine signifikante Abweichung der rekonstruierten Winkel zu beobachten ist.

Abstract

This work investigates how a Gamma Ray Burst analysis with the neutrino telescope Antares can be performed. Gamma Ray Bursts are short and very intense flashes of high energy Gamma rays, which occur totally unpredictably on the sky. Within timescales of only seconds, they release as much energy as the Sun in its whole lifetime. A subclass of GRBs is nowadays widely believed to be associated with a certain type of supernovae, which end with the formation of a black hole. The observed electromagnetic radiation can be explained by highly relativistic outflows of material, most likely collimated in jets, which are by chance pointed towards the Earth. When these ejecta are slowed down, shock fronts emerge, in which electrons are accelerated. The prompt γ–Ray radiation is due to the synchroton emission of the highly relativistic electrons. Among the electrons, also protons are assumed to be shock–accelerated, which would result in the emission of high energy neutrinos accompanying the electromagnetic signal of the burst. The detection of Gamma Ray Burst neutrinos would be an unambiguous proof for the assumption of hadronic acceleration in cosmic sources and could serve to explain the Cosmic Ray flux at ultra high energies.

In this work, a strategy for a possible GRB analysis with the Antares experiment using Monte Carlo simulated data is being investigated. In principle, the analysis is applicable for all bursts, but it is performed exemplary for GRB080218B. The Monte Carlo simulations are adjusted in order to represent the burst's expected neutrino flux and to simulate the detector at the respective time. To provide a preferably realistic analysis, real optical background collected at that time is added to the simulated files. The analysis is optimized in order to yield highly significant discoveries when applying it to the real data.

In addition, a method to correct for systematic errors in the angular reconstruction is being investigated. Using Monte Carlo simulations of some particle tracks in the detector, I examined the appearance of significant shifts of the reconstructed angles with respect to the original Monte Carlo directions. The existence of such systematic deviations could be shown. This allows for an event–by–event correction of the angular reconstruction, thereby improving the angular resolution of the detector.

CONTENTS

1. Introduction

For a long time, light has been the only messenger to study the Universe. Only recently, new experimental techniques have been developed, which opened new possibilities to investigate the cosmic radiation in all its different energy ranges and components: From X- and Gamma-Rays up to Cosmic Rays, Gravitational Waves and even high energy cosmic neutrinos.

Neutrinos are a very promising messenger from the sky: Since they only weakly interact with matter, they even can escape from very dense regions of the Universe. And as they do not carry any charge, they are not affected by magnetic fields. Hence a neutrino signal directly points towards its source. But the big advantage of neutrinos, the weak interaction with matter which allows them to travel undeflected and unabsorbed through the Universe, turns into a big disadvantage when trying to detect them. They cannot be observed directly, but only via detection of interaction products. Because of their very small cross sections, an enormous amount of detection material is needed in order to attain a reasonable number of interactions.

1.1. Gamma Ray Bursts

Gamma Ray Bursts are surely among the most fascinating and powerful, yet still mysterious sources in the Universe. As their name suggests, they are brief and intense flashes of high energy γ–Rays, which occur totally unpredictably on the sky. The enormous energy output in very short time scales turns them into the most powerful explosions in the Universe. In only a few seconds, Gamma Ray Bursts emit as much energy as the Sun in its whole lifetime. The short prompt emission is often followed by a fast fading afterglow emission at lower energies. It can be observed for example in X–Rays, the optical and the radio regime and can last up to a few days or weeks after the burst. For their very short lifetime, GRBs are the most luminous Gamma–Ray sources in the sky which outshine the whole rest of the γ–Ray sky. But still, due to their short durations no detailed study was available for a long time.

The first bursts were discovered 'accidentally' in 1967 by U.S. Vela satellites — dedicated to detect secret nuclear weapon tests on Earth. But the observed short flashes of MeV photons did not match any known nuclear weapon test signature. Sixteen short high energy bursts were observed by the Vela satellites in a period of three years (Klebesadel et al., 1973), lasting between 0.1 and 30 s. Fluences between 10^{-5} and $2 \cdot 10^{-4}\,\mathrm{erg/\,cm^2}$ were measured. As each of the bursts was observed in at least two of the four satellites, rough estimations of the sky positions could be made which definitively ruled out terrestrial or solar origin of the bursts (Klebesadel et al., 1973).

It was not until 1991, when the Compton Gamma Ray Observatory with its Burst and Transient Source Explorer (*BATSE*) on board was launched, that the unpredictable flashes

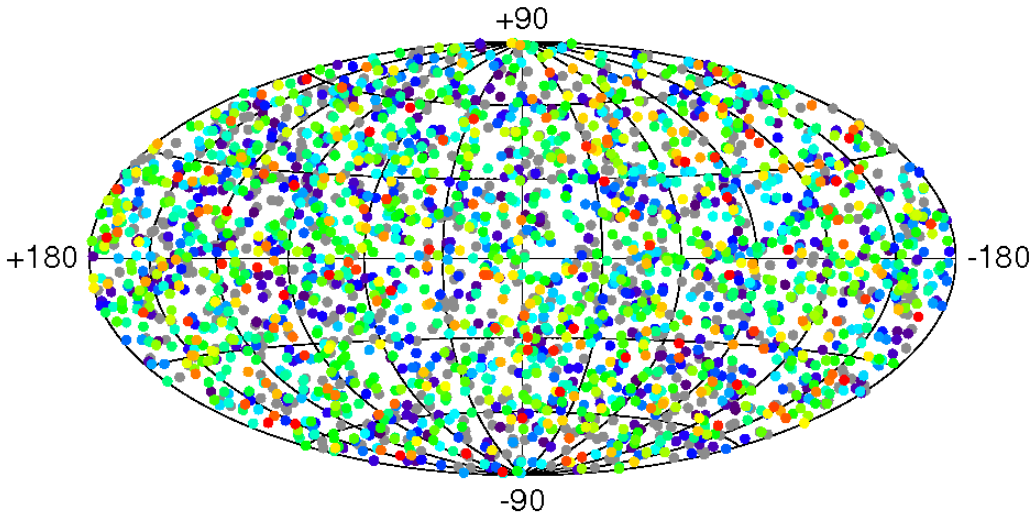

Figure 1.1.: The sky map of the 2704 bursts detected by BATSE between 1991 and 2000 in galactic coordinates. They are uniformly distributed on the sky, indicating their origin to be either in our closest vicinity or outsides the Milky way. Together with the first afterglow measurement in 1997 (Metzger et al., 1997), the cosmic origin of the bursts could be confirmed. (available at `http://www.batse.msfc.nasa.gov/batse/grb/skymap`*)*

of γ radiation could be investigated further. *BATSE* was especially designed for the investigation of Gamma Ray Bursts. Its detection of roughly 3000 bursts within nine years gave new insights and allowed for systematic studies of the sources. The burst were found to be isotropically distributed on the sky (Meegan et al., 1992), which strongly points toward the cosmic origin of GRBs (see fig. 1.1). Furthermore, the measurements revealed a wide variety of durations, intensities and time profiles of the bursts.

The duration of a GRB is usually given as the time period T_{90}, in which 90% of the photons are detected. *BATSE* could observe durations between 30 ms and more than 1000 s. The distribution of burst durations as shown in fig. 1.2 exhibits a double peaked structure, which led to the classification of bursts into two types (Kouveliotou et al., 1993; Paciesas et al., 1999):

The short bursts, which are usually harder in spectrum, with a duration shorter than 2 s and the long GRBs with $T_{90} \gtrsim 2\,\mathrm{s}$, showing in average softer spectra — i.e., the spectrum falls steeper at higher energies. These differences in the observed spectra and light curves speak for the existence of two separate populations of Gamma Ray Bursts.

But for a better understanding of the bursts, longer observation times were necessary. This could only be realized by measuring the fast decaying emission of a long burst in other wavelengths, the so–called afterglow. Since this radiation fades fast, the notification of a burst occurrence would have to be distributed instantaneously to Earth-based telescopes. To allow them to rapidly point towards the GRB direction, the respective sky position of the burst has to be known accurately.

BATSE could reveal the isotropic occurrences of the bursts, but its angular resolution of only 2° did not allow for fast follow–up observations of the rapidly fading afterglow. A new satellite called *BeppoSAX* was launched in 1996, which could localize the bursts to a

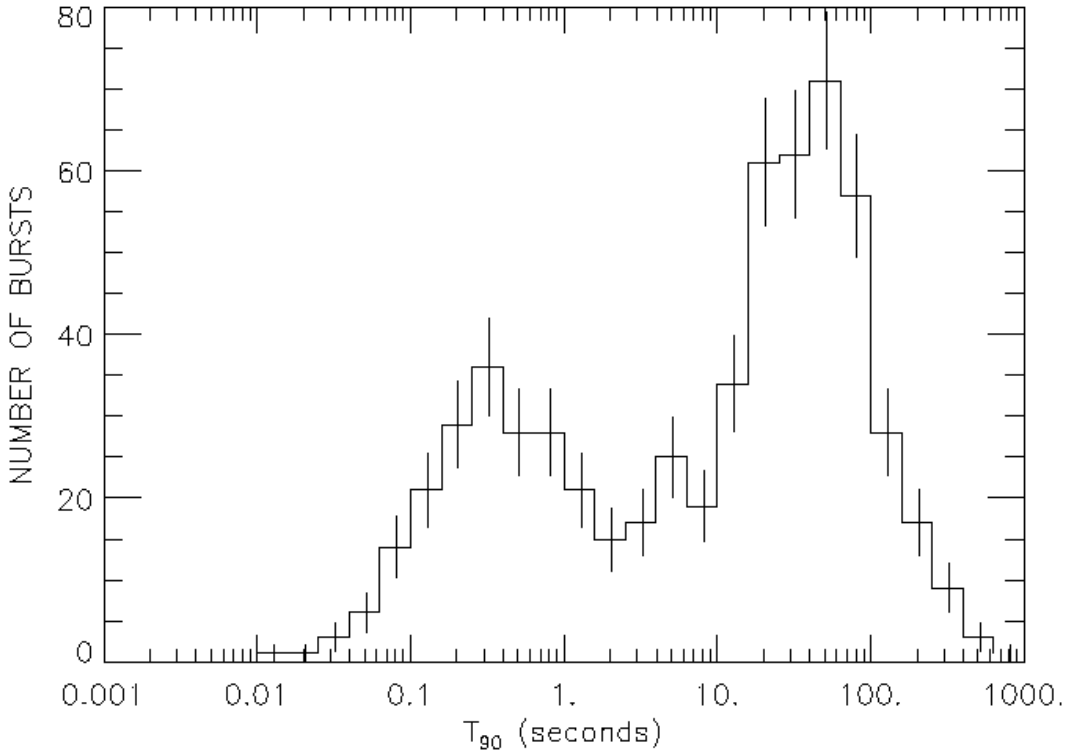

Figure 1.2.: The distribution of the burst duration as measured by BATSE . This double peaked distribution led to the classification of GRBs into two types, separated at roughly 2 s. *(Paciesas et al., 1999, available at* `http://www.batse.msfc.nasa.gov/batse/grb/duration`*.)*

precision of $\sim 3'$. The fast distribution of the GRB notifications allowed to measure the afterglow emissions of GRBs for the first time (Metzger et al., 1997). Measuring the spectral features of the optical counterpart is a powerful tool to determine the distance of the source. When absorption and emission lines of certain elements or isotopes can be identified, their shift with respect to the original line energy directly reflects the cosmological redshift z of the source. In 1997, 25 years after the first GRB observation, afterglow emission with optical counterpart could be observed for the first time (Metzger et al., 1997). This allowed for the identification of a very faint host galaxy and measurement of the first redshift: GRB970508 was found to be at $z = 0.835$, i.e., 6 billion lightyears away from Earth. Further measurements of the redshifts placed the bursts at cosmological distances, at redshifts up to even $z \sim 6$ (Fiore et al., 2006).

The long distances immediately implicated an enormous total energy output of $\sim 10^{52}$ erg[1] and even more. Since this large amount of energy is released in timescales of only seconds, GRBs are the most luminous objects ever observed in the Universe.

In 1998, the detection of GRB980425, which was directly followed by a Supernova (SN 1998 bw), implied a strong relationship between GRBs and the death of very massive stars (Galama et al., 1998; Woosley & Bloom, 2006). This connection was further encouraged by more and better position measurements of long bursts, which placed them within star forming regions. Today, it even seems to be possible to use long bursts as a tracer to probe

[1]Under the assumption of isotropic emission.

high redshift star formation (Fiore et al., 2006). Nowadays, it is well–established that long GRBs originate from core collapses of very massive and fast rotating stars in so–called hypernovae (see, for instance, Woosley & Bloom, 2006, and references therein.). For the short bursts of $\lesssim 2\,\mathrm{s}$ duration, it is much harder to measure afterglows and gain more information about their origin, but their occurrence does not seem to be constrained to star birth regions. It is now widely accepted that they originate from merging of two compact objects, namely neutron stars and black holes into one black hole (Eichler et al., 1989).

In both the long and the short Gamma Ray Bursts, the underlying processes to produce the total energy output of up to $\sim 10^{52}\,\mathrm{erg}$ is not yet fully understood, but there are plenty of models which try to explain the powerful physics underneath. The rapid variability in the order of milliseconds implies very compact sources, which thus have to show enormous photon densities. This feature first seemed to contradict the observation of γ rays up to GeV, since such a compact source should have a huge optical depth. Photons of energies $\gtrsim 500\,\mathrm{keV}$ should rather produce e^+e^- pairs than escape the emission region. Yet still, the clearly non–thermal spectra indicate optically thin sources. This problem — known as the compactness problem — could only be overcome if the emitting regions would move at highly relativistic velocities of $0.9999\,\mathrm{c}$ and larger towards the observer (see, e.g., Piran, 1998). Because of the relativistic beaming effect, the photons would be observed at higher energies than with which they were emitted. Furthermore, the size of the emission region would appear smaller.

Nowadays, it is often believed that GRBs are in one way or another associated with the formation of a black hole (Piran, 1998). This inner engine seems to power highly relativistic outflows, most probably collimated in jets. When these ejecta are slowed down, shock fronts emerge. The dissipation of kinetic energy into internal energy in the shocks produces the high energetic prompt emission.

Internal shocks may arise from inhomogeneities within the outflow, for instance from several ejected shells which were ejected at different velocities. The collision of the ejecta with the ambient medium causes external shocks. Therein, electrons are being Fermi accelerated up to ultra relativistic energies when passing the shock fronts. The synchroton emission of these electrons and inverse Compton scattering of the emitted photons causes the observed GRB radiation. It is assumed that the outflow does not exclusively contain electrons, but also baryons (Waxman, 1995a, 2000). All charged particles present in the ejecta should be Fermi accelerated in the shocks. Protons may be accelerated to energies $\gtrsim 10^{20}\,\mathrm{eV}$, which might serve to explain the Ultra High energy Cosmic Ray flux (UHECR). Waxman (1995b) showed that if protons were as efficiently accelerated as electrons, the spectrum and flux expected from Fermi acceleration in cosmological GRBs is consistent with that of the UHECR at $\gtrsim 10^{19}\,\mathrm{eV}$. If protons were Fermi accelerated together with the electrons, high energy neutrinos would be expected to accompany the synchrotron and inverse Compton γ–rays. Waxman & Bahcall (1997) found that the interaction of the accelerated protons with the γ-Rays would result in a burst of $\sim 10^{14}$ Gamma Ray Burst neutrinos via photo–meson production.

Based on this assumption, neutrino telescopes are searching for the neutrino signal from Gamma Ray Bursts, which could give further insights into the underlying processes and confirm the baryonic acceleration assumption.

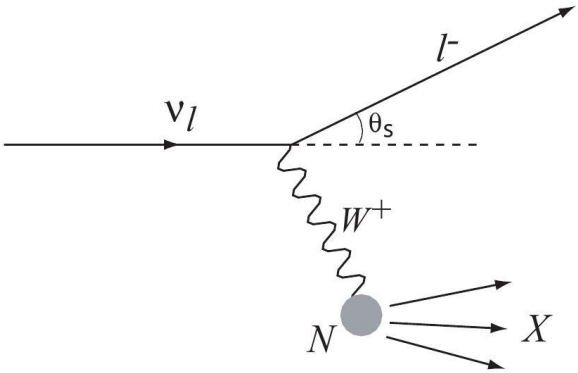

Figure 1.3.: The charged current interaction of a neutrino ν_l with a nucleus. The produced lepton l^- produces Čerenkov light when travelling through a medium faster than the respective speed of light in that medium. (Bouwhuis, 2005)

1.2. NEUTRINO DETECTION

As mentioned above, neutrinos are a very promising messenger to study astrophysical processes: Because of their uncharged nature, they are not deflected by matter and electromagnetic fields travelled through on their way to Earth. Hence they point directly to their location of production. Their extremely low interaction cross section, on the other hand, allows them to travel large distances and pass large amounts of matter without being absorbed. Consequently, even the densest regions in the Universe could be observed in the 'light' of neutrinos.

But it is their very low cross section that makes the detection of neutrinos so challenging — large detectors with tons of detection material are needed in order to have a chance to see these only very weakly interacting particles. One way to detect high energy neutrinos is to observe the charged secondary particles from a reaction of the neutrino with the detector medium. For involved energies greater than $\sim 1\,\mathrm{GeV}$, the interaction product may fly faster than the speed of light in the medium. In this case, it emits so–called Čerenkov light on its way through the detector. From the detection of the Čerenkov photons, directional information of the primary neutrino can be reconstructed.

A neutrino can only interact with matter via the weak force, exchanging either a charged W-boson in a charged current interaction (CC) or a Z-boson in a neutral current interaction (NC):

$$\text{CC–interaction:} \quad \nu_l + N \longrightarrow l^- + X \tag{1.1}$$
$$\overline{\nu_l} + N \longrightarrow l^+ + X$$
$$\text{NC–interaction:} \quad \nu_l + N \longrightarrow \nu_l + X \tag{1.2}$$
$$\overline{\nu_l} + N \longrightarrow \overline{\nu_l} + X$$

The CC–interaction, illustrated in fig.1.3, of a neutrino ν_l hitting an atomic nucleus N produces a charged lepton l^- and a shower of hadrons X when the nucleus breaks up. The lepton l can either be an electron, muon or tau–particle, depending on the type of the primary neutrino. As we will see later on, ν_μ are the most suitable neutrino candidates for

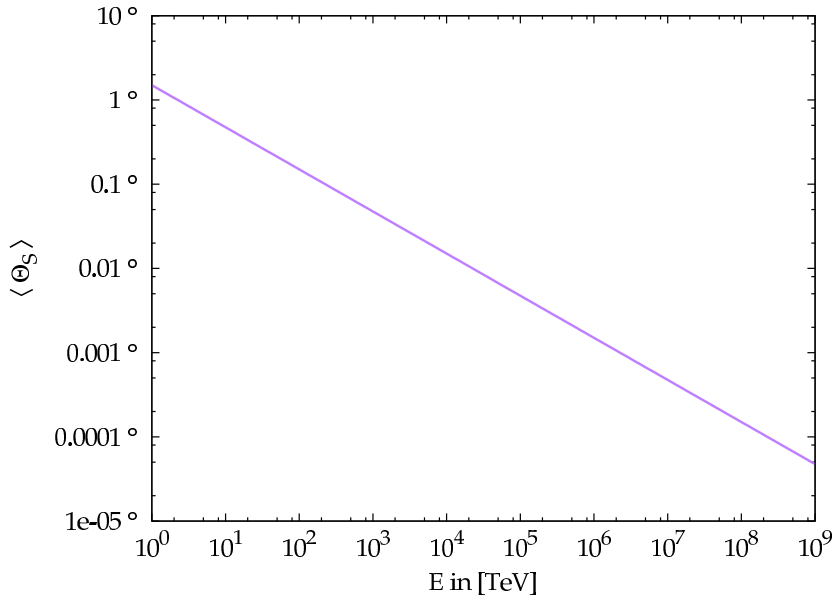

Figure 1.4: The average scattering angle $\langle\Theta_S\rangle$ between the initial ν_μ and the produced muon direction. For high energies, the two particles are nearly aligned.

detection. The scattering angle Θ_S between the incoming neutrino and the charged lepton l depends on the transferred momentum. On average, half of the neutrino momentum is transferred onto the lepton[2] (Bouwhuis, 2005). For high energies, the angular spread of the lepton direction with respect to the primary neutrino becomes smaller, typically $\Theta_S \lesssim 1.5° / \sqrt{E_\nu[\,\mathrm{TeV}]}$ (Bouwhuis, 2005).

Hence the lepton and the primary neutrino are virtually aligned at high energies. This is a big advantage for neutrino telescopes, since by reconstructing the lepton track, the original neutrino direction can be obtained. Figure 1.4 presents the dependency of the mean scattering angle on the neutrino's energy.

1.3. THE ANTARES DETECTOR

The ANTARES neutrino telescope is primarily designed to detect the charged leptons from CC-interactions of neutrinos with matter (see eq. 1.1). It is located in the Mediterranean Sea at a depth of 2.4 km. The detector consist of 12 vertical strings, anchored on the seabed and held upright by a buoy at the top. They are separated from each other by a typical distance of $\sim$60 m. The 12 lines with a length of $\sim$500 m each are equipped with triplets of photo multiplier tubes (PMTs), building a 3–dimensional array of 900 PMTs in total. The 25 triplets of PMTs along one line — called storeys — have a vertical distance of 14.5 m from each other, whereas the first storey is placed in a height of 100 m above the seabed. The instrumented volume is $\sim 0.02\,\mathrm{km}^3$. A schematic view of the detector is given in fig. 1.5.

1.3.1. DETECTION PRINCIPLE

ANTARES is constructed to detect neutrinos indirectly, using the seawater in and around the instrumented volume as detection medium. When an upgoing neutrino interacts with the rock or water under the detector via CC–interaction (see eq. 1.1), charged relativistic

[2] 3/8 for the anti-neutrino

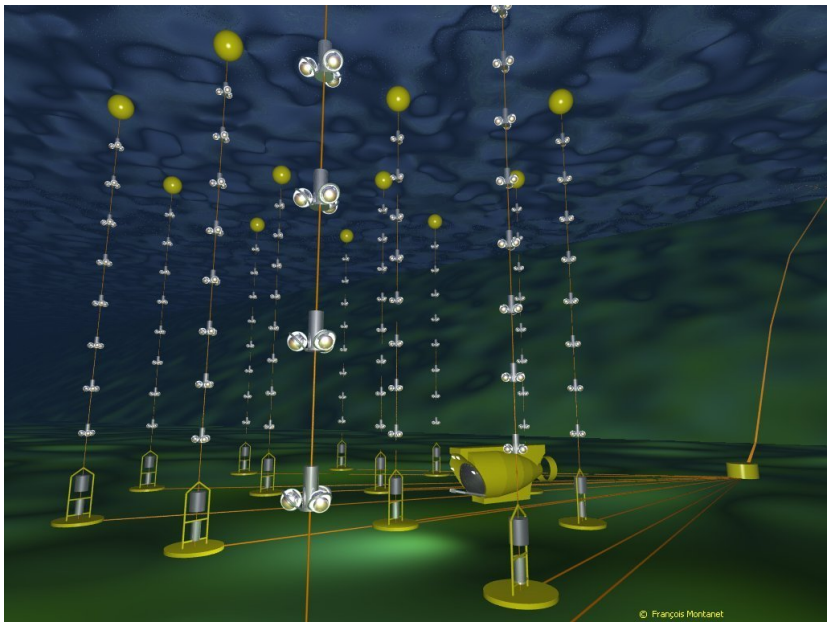

Figure 1.5: A schematic view of the ANTARES *detector.*

particles are produced. If the speed of these particles travelling through the medium exceeds the speed of light of that medium, they produce an electromagnetic shock wave, the so–called Čerenkov light. This coherent radiation consisting of UV and optical photons is emitted in a cone with characteristic angle Θ_C around the particle direction:

$$\cos\Theta_C = \frac{1}{\beta n} \tag{1.3}$$

with β being the speed of the particle[3] and n being the refraction index of the medium. For relativistically travelling particles in seawater ($n = 1.35$), the Čerenkov angle is $\Theta_C = 42.5°$. The emitted Čerenkov light is detected by the photo multiplier tubes.

The propagation of the Čerenkov light to the PMTs is affected by the absorption and scattering probabilities of the seawater (see, e.g., ANTARES Collaboration, 2005). At the detector site, the absorption length λ_{abs} is about 60 m and the scattering length is 260 m for light of wavelength $\lambda = 460$ nm. The intensity of the Čerenkov light decreases with the travelled path r of the photon:

$$I(r) \propto \frac{1}{r} e^{-\frac{r}{\lambda_{abs}}} \tag{1.4}$$

The intensity and arrival times of the photons eventually detected by the PMTs also depend on the light scattering. The light dispersion introduces a slight spread in the arrival times of $\sim 1 \ldots 2$ ns after a distance r of 100 m. The probability of light scattering up to even high scattering angles can cause a delay of up to a few 100 ns (ANTARES Collaboration, 2005).

1.3.2. INTERACTION SIGNATURES

Depending on the type of the primary neutrino, the interaction products of the CC interaction eq. (1.1) produce different signatures, either a shower or a track. Showers are

[3] In units of the speed of light, $v = \beta / c$

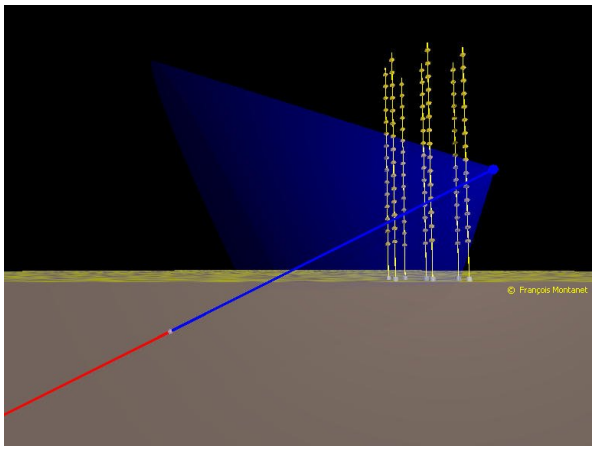

Figure 1.6: The principle of detection of the ANTARES *neutrino telescope. The upgoing neutrino is drawn in red. It interacts with the rock under the telescope, where a muon is produced. The muon and its Čerenkov light cone are drawn in blue.*

produced if the interaction length of the particles is very small, i.e. the particles travel only short distances before interacting again, which produces new particles.

If, on the other hand,the interaction length is long with respect to the spacing between the detector devices, the particle travels undeflected through the medium leaving a long straight line, called a particle track.

At sufficient high energies, the particles emit Čerenkov light[4], which can be detected by the PMTs.

HADRONIC SHOWER At the interaction vertex of both CC and NC interactions, the target nucleon breaks up and produces hadrons. Because of the high energies, many of the charged particles produce Čerenkov light. After a mean interaction length of 80 cm, the hadrons will interact with the detection medium and the process repeats. After a few interaction lengths, the energy of the particles will eventually drop below the threshold for Čerenkov light emission. Due to the short interaction length with respect to the separation of the PMTs in ANTARES (the vertical distance of the storeys, for example, is 14.5 m), hadronic showers only produce very local light signals in the detector.

ν_e INTERACTION The interaction of an electron neutrino with matter produces an electron, which very efficiently loses its energy via bremsstrahlung. The emitted photons themselves will produce e^-e^+–pairs and the process is iterated, which leads to an electromagnetic shower. Since the radiation length in water is 36 cm and the Čerenkov light emission is limited to only a few radiation lengths, the size of the electromagnetic shower is again very small compared to the spacing of the PMTs. Consequently, ν_e interactions can only be detected for interaction vertices very close or inside the detector and cannot be used for directional reconstruction.

ν_μ INTERACTION For the muon with its relative high mass compared to the electron, bremsstrahlung emission is strongly suppressed. Since it loses only very little energy (typically $\sim 0.2\,\mathrm{GeV/m}$), it can travel long distances with relativistic speed, still emitting Čerenkov light. The Lorentz boost dilates the very short rest frame lifetime of 2µs , so the

[4]The Čerenkov threshold can be derived by eq. 1.3, since $|\cos\Theta_C| \leq 1 \longrightarrow \beta \geq 1/n$, i.e., the particle travels faster than the speed of light in the medium.

muon can travel long distances in water: a 100 GeV muon, for instance, can travel around 500 m (Bouwhuis, 2005). For higher energies, the travelling distance increases up to even kilometres. The scattering of the muon in water is very small compared to the scattering angle Θ_S between muon and the primary neutrino.

ν_τ INTERACTION The τ particle produced by a primary ν_τ has a very short lifetime of only $3 \cdot 10^{-13}$ s. This corresponds to a travelling distance of ~ 100 m in the detector, before it decays and produces a hadronic shower. This is still short compared to the distances a muon can travel. In 17% of the decays a muon is produced, which leads to a signature as described above. So the tau–neutrino will in principle induce two hadronic vertex showers, separated by ~ 100 m. The second shower might be followed by a muon track.

Because of the different signatures of the interaction products, the muon neutrino with the long straight muon track is the most suitable candidate for neutrino detection. By reconstructing the muon track from the Čerenkov signal in the PMTs, directional information about the original neutrino can be obtained.

1.3.3. BACKGROUND

In order to do astronomy, ANTARES is looking for signals from cosmic ν_μ interactions. But beyond that, there are other processes which can produce muon tracks in the detector and are considered as background to the cosmic neutrino signal. Air showers, for example, are generated when high energy cosmic rays hit the Earth's atmosphere. In these showers, all kinds of particles are produced — among them, the so–called atmospheric muons and neutrinos. Since only the weakly interacting neutrinos are capable of traversing the Earth unaffected, the Earth can be effectively used as a 'shield' against all particles but the neutrino flux. So by only searching for upgoing particles, the atmospheric μ background can be effectively reduced. But still, also muons from above can produce signals in the detector, for instance from scattered light. Up to now, falsely reconstructed atmospheric muon tracks pose a significant challenge.

Atmospheric neutrinos produced by cosmic rays below the horizon can also traverse the Earth and represent an irreducible background to the signal cosmic neutrinos. These neutrinos will in average have lower energies. But still, whether a detected upgoing muon was produced by an atmospheric or cosmic neutrino cannot be distinguished on an event by event basis.

Another background component in the PMTs is due to bioluminescence and radioactive decay of ^{40}K in the seawater (ANTARES Collaboration, 2000). This more or less random optical background can vary between 50 and 300 kHz, depending for example on the time of the year or the sea current. A dedicated trigger is implemented in the ANTARES data filter which records this optical background. Every 10 seconds, all incoming raw data is being stored for 4400 ns without any further filtering. These data are called 'minimum bias data' and is used to estimate the current background in the detector.

1.3.4. MONTE CARLO SIMULATION

In order to understand and examine the various effects on the way from the primary neutrino up to the detection of the neutrino signal in the detector, a set of software tools is available to simulate the underlying processes. These programs simulate incoming primary neutrino fluxes in the energy range of 10 to 10^7 GeV. The transmission probability of the particles through the Earth depends on the respective zenith angle, which determines the column density of matter the neutrino has to pass, and its energy. In the vicinity of the instrumented volume, the neutrinos might finally interact with the rock or seawater. The interaction and the propagation of the produced particles through the medium is being simulated — especially the propagation of the muon from a ν_μ interaction through the seawater. If the muon reaches a certain region around the instrumented volume, the Čerenkov light emission and propagation is simulated. This cylindrical volume of radius $r = 266.11$ m around the detector to which the Monte Carlo light production and propagation is limited is called the can. The Čerenkov light produced by particles outside the can cannot reach the instrumented volume and thus cannot be detected by ANTARES. The absorption, scattering and light dispersion of the photons in water are also taken into account. The characteristics of the PMTs — e.g. the quantum efficiency and the effective area of the photocathode — determine the actual digital signal as detected when one of the photons hits a PMT.

Several programs are available for Monte Carlo simulations in ANTARES : Neutrinos are simulated by GENHEN, which calculates the propagation of the particles to the can. The programs MUPAGE, CORSIKA and FLUKA simulate the atmospheric muon background. The detector response including Čerenkov light emission of particles within the can is simulated by KM3.

In an analysis like the GRB investigation with ANTARES, certain blinding policies have to be respected in order to optimize the analysis in an unbiased way but still yielding for an statistically significant discovery when unblinding the data. Monte Carlo simulations are a powerful tool in this context, as the information of the origin of an event is still known and can be compared to the outcome of an analysis, for instance the reconstructed particle direction or whether the track originated from background or signal flux.

The Monte Carlo (MC) data set used in this analysis was produced in the so–called *Bari–Valencia production* (see Bailey, 2002a, for a description.). These neutrino events represent the atmospheric neutrino flux according to the *Bartol model* (Barr et al., 2004). The very same data set is used to determine the GRB spectrum, which will be explained in section 3.2.2.

1.3.5. ANTARES LOCAL COORDINATES

The local coordinate system of the detector is defined by the two angles Zenith Θ and Azimuth Φ. The Zenith angle describes the angle between the particle track and a vertical line through the ANTARES detector. The Azimuth accounts for rotation around the vertical axis. For illustration, the coordinate system is given in fig. 1.7. The particles coming from below the ANTARES detector are referred to as upgoing. An exactly upgoing particle flying vertically through the detector corresponds to $\Theta = 180^\circ$. Note that both Zenith and Azimuth denote the direction of the particle's origin, not the direction in which it is flying.

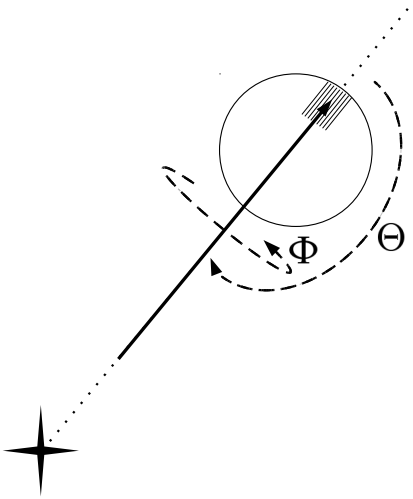

Figure 1.7: The local coordinate system for the ANTARES *detector. Signals from Zenith angles $\Theta > 90°$ are called upgoing. The Azimuth angel Φ takes account for the rotation around the vertical axis of the detector.*

1.3.6. THE SOFTWARE FRAMEWORK SEATRAY

In a detector like the ANTARES neutrino telescope, the transformation of raw data into physics information is a very complex task. This is the reason why in high energy physics, it is commonplace to modularize the very complex data processing into small functionality units, being preferably independent of each other. Within the ANTARES collaboration, a software framework called SEATRAY is available (see Eberl & Kopper, 2009, for a description). The framework itself is written in the coding language C++, the steering file is commonly implemented using the PYTHON scripting language.

The functionalities are provided by modules with exactly defined interfaces. Data is passed from one module to the next in data containers called *frames*. Each of these frames describes a single detector event. Within the frames, data is stored using name–object tuples, containing for example a mapping of the detected hits from Čerenkov photons onto the respective optical modules. The modules can use so–called *Services*, which provide common tools used within the framework. During the data analysis, the modules can modify the passing frames, read out the tuples or add information. No constraints are imposed on the information to be stored in the frames.

1.4. THIS WORK

Due to their short duration and their occurrence at accurately defined sky positions, Gamma Ray Bursts are very favourable objects for analyses with neutrino telescopes like ANTARES. The confinement to very small angular search cones and time windows in the order of seconds reduces the background very efficiently.

This work focusses on optimizing the analysis of Gamma Ray Bursts with the ANTARES neutrino detector.

One of the most favoured models — the fireball model — for Gamma Ray Bursts is reviewed in chapter 2, including the calculation of the expected neutrino spectrum given

in section 2.4.

For the further investigation, I selected a sample of suitable GRBs with the highest expected neutrino fluxes, which produced upgoing signal in the detector. The ANTARES data taking conditions have also been taken into account in the selection. The procedure is described in section 3.1.

To simulate the neutrino flux of a burst, Monte Carlo event files are being adjusted in order to represent the GRB signal (see section 3.2). For a preferable realistic analysis, real optical background of the respective GRB time was added to the Monte Carlo events. The calibration of the actual Gamma Ray Burst occurrence was applied to the data set before reconstructing the event files with the so–called AART STRATEGY.

After that, the resulting expected signal and background flux can be calculated. The ratio of these two fluxes can be influenced by cutting on certain parameters like the quality parameter of the event reconstruction Λ, the angular cone around the Gamma Ray Burst direction and the number of hits an event triggered in the detector. This set of cut parameters is optimized in order to yield high significance for discoveries (see section 3.3). The results are summarized in section 3.4.

Furthermore, the feasibility of a new method for event–by–event correction of angular reconstruction was investigated (chapter 4). It might be possible that apart from statistical errors in the reconstructed angle distributions, also systematic errors could contribute and worsen the reconstruction algorithms. These could, for instance, arise from the actual track position and orientation relative to the detector devices. If such systematic shifts would be known, they could in principle be corrected on an event–by–event basis.

2. Gamma Ray Bursts

2.1. The Fireball Model

The occurrence of long GRBs only within star birth regions strongly implies their correlation with the death of the most massive and fast rotating stars (see, e.g., Woosley & Bloom, 2006, and references therein.). At the end of their stellar evolution, stars with masses $\gtrsim 20 \ldots 30 M_\odot$ evolve into very hot Wolf–Rayet stars (see fig. 2.1) with strong stellar winds. After a relatively short lifetime, these stars eventually explode in Supernovae of type I b/c, which are sometimes referred to as 'Hypernovae' because of the very high mass of the progenitors (see, e.g., Piran, 1998; Woosley & Bloom, 2006). Very energetic gamma radiation of up to $\sim 10^{52}$ erg in total[1] is being emitted in only a few seconds. The variability Δt of the photon emission on timescales of microseconds limits the emitting region to a very small size of $r_0 \sim 10^7$ cm (Waxman & Bahcall, 1997). The observed luminosities of 10^{51} erg/ s within such compact sources imply a very dense and thus optically thick plasma. From this plasma, photons with energies above ~ 1 MeV should not be able to escape because of $e^- e^+$–pair–production. This opaque plasma of e^-, e^+ and γ is called fireball (Piran, 1998).

The observed non–thermal spectrum, on the other hand, requires an optically thin source. Goodman (1986) and others realized, that this compactness–problem could be overcome if assuming highly relativistic motion of the source towards the observer. They showed that only if the γ emitting region would expand with ultra relativistic speeds, the observed high energy photons could be explained. From the hardness of the spectra, Lorentz factors $\Gamma \sim \mathcal{O}(100)$ can be deduced. Relativistic beaming effects would on the one hand reduce the required photon energy at the source of a factor of $1/\Gamma$, so presumably under the threshold for $e^- e^+$–pair–production. On the other hand, the actual radius of the source could be larger by a factor of Γ^2 (Piran, 1998).

The relativistic motion towards the observer must not necessarily originate from the source itself — in fact, that would be rather unlikely — but can just be explained by relativistic expansion of shells or jets, ejected from the inner engine. The relativistic beaming allows the observer to only see the radiation from a cone of $1/\Gamma$ around the line of sight. Thus by pure observation, it cannot be distinguished whether the radiation is collimated in a jet or emitted spherically. But the large amount of emitted energy of up to 10^{52} erg (if isotropic emission is assumed) makes the assumption of isotropic emission questionable[2] (Rhoads, 1997). Hence, to reduce the total energy output of a burst, a collimated outflow into a small solid angle seems to be more realistic. This would reduce the total output by a factor of $\Theta^2/4\pi$ for a collimated outflow with opening angle Θ (Rhoads, 1997).

The required relativistic motion arises naturally from the release of a large amount of

[1] The energy output requires the measurement of the redshift of the source. From the distance and the observed luminosity, the total energy output can be deduced when assuming isotropic emission.

[2] Compare, e.g., the energy output of the Sun, 10^{41} erg/ year!

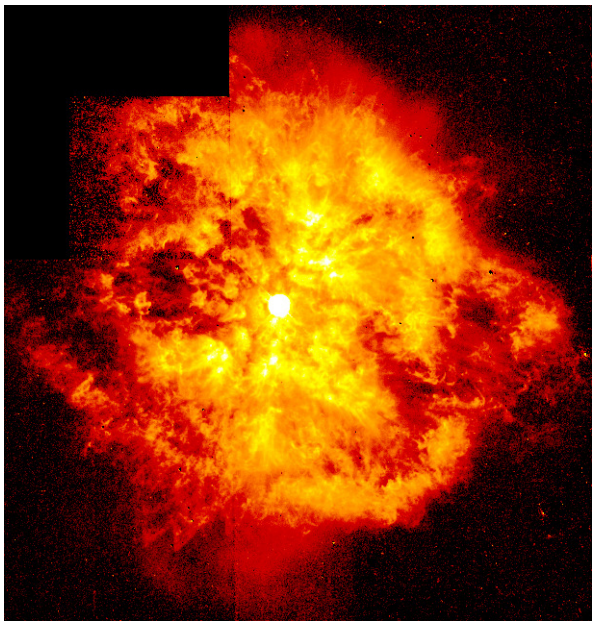

Figure 2.1: Hubble Space Telescope image of the Wolf–Rayet star WR 124. These most massive stars are considered as the progenitors of long Gamma Ray Bursts. (picture courtesy NASA/ESA.)

energy in a small volume. The large optical depth leads to the formation of a photon–pair–fluid with very high pressure (Piran, 1998). This over–pressured fireball then expands relativistically under its own pressure until the photons can escape. Goodman (1986) could show that a pure radiation fireball of only γ and $e^{\pm}$ would release all photons at once when becoming optically thin. This would result in a thermal spectrum, in contrast to the non–thermal spectrum that is observed. Shemi & Piran (1990) showed that if the fireball on the other hand contained only a small amount of baryonic matter, the observed non–thermal spectrum can be explained (see, for example, Shemi & Piran, 1990; Waxman, 2000).

When this relativistically moving shell — or, more likely, jet — is slowed down, the kinetic energy is being converted into internal energy (Rees & Meszaros, 1992). This process causes the observed release of radiation up to GeV γ–Rays from synchrotron emission of relativistic electrons and inverse Compton. This can occur in either internal shocks from irregularities in the outflow, or in external shocks, when the ejecta crash into the surrounding medium. That may be the formerly ejected stellar wind, or the interstellar medium (ISM) (Piran, 1998). The accepted model is that the high energy GRB prompt emission is caused by the internal shocks, followed by the afterglow emission from the interaction of the ejecta with the ISM. Note that in both cases, the flow needs to be optically thin to allow the photons to escape. So both the prompt and the afterglow emission are being radiated at large radii from the source, allowing for a non–thermal emission (Piran, 1998). Since the radiation is only due to the slowing down of the ejecta, the inner engine remains unknown and unseen.

The measured light curves of Gamma Ray Burst afterglows contain strong evidence for the relativistic fireball model. The light curves can — as well as the energy spectra — be parametrized as power–laws with different regimes (Mészáros, 2006; Sari et al., 1998). Note that since the GRB is most likely due to a jet pointed towards the Earth, the actual rate of GRBs is supposed to be much higher. Modern detectors like *Swift* detect $\sim$300 bursts per day. They occur at a rate of only a few per galaxy in 10^6 years.

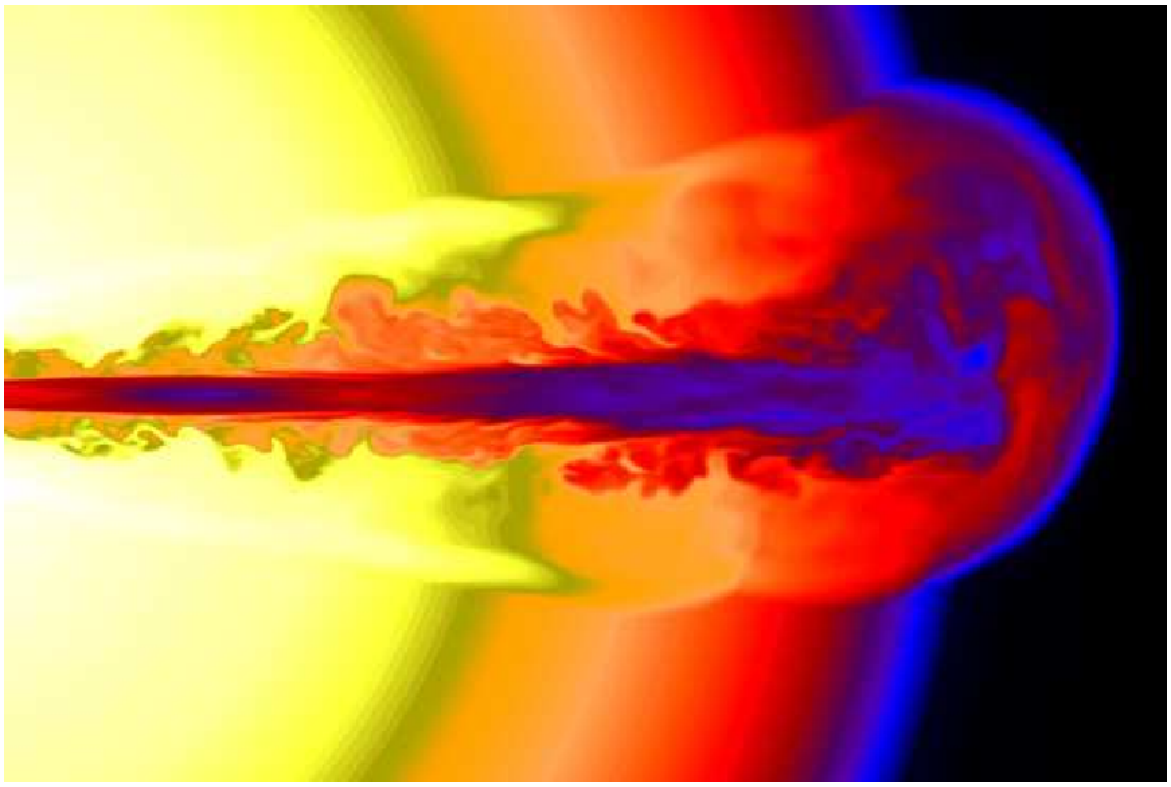

Figure 2.2.: Simulation of a density profile of a relativistic GRB jet, breaking out of a $15M_{\odot}$ *Wolf–Rayet star,* $\Gamma \sim 200$*. From Woosley & Bloom (2006)*

2.2. THE SHOCK MODEL

In collisions within the relativistic ejecta, or interaction of the ejecta with the surrounding medium, shocks emerge which are capable of accelerating charged particles up to ultra relativistic speeds (Piran, 1998; Longair, 1994). Every time the particles pass the shock front, they experience a slight energy gain ΔE. Inhomogeneities in the magnetic field in and around the shock may reflect the particles, causing them to pass the shock front several times, each time gaining a little energy. This process is called Fermi shock acceleration. It can be shown that many particles undergoing this process finally produce a power–law spectrum $\frac{dN(\epsilon)}{d\epsilon} \propto \epsilon^{-p}$ with $p \gtrsim 2$ (The mechanism is described in detail in Longair, 1994). The resulting observed photon emission is due to Synchrotron and inverse Compton emission of the ultra relativistic e^- (Waxman & Bahcall, 1997; Rees & Meszaros, 1992).

The strong variability of the prompt γ–emission cannot be explained by the interaction with the ambient medium. These external shocks would be smooth and would not show any temporal structure (Sari & Piran, 1997; Piran, 1998) — so the external shocks with the ISM are more likely to produce the observed smooth afterglow radiation, whereas the strongly variable prompt emission can be explained by internal shocks.

2.2.1. INTERNAL SHOCKS

Internal shocks may arise from inhomogeneities in the relativistic ejecta or collisions of shells which are moving outwards at different speeds. Internal shocks are produced, where electrons are Fermi accelerated up to ultra relativistic energies. These electrons emit γ–Rays, giving rise to the observed prompt GRB radiation on timescales of $\delta t \sim$ ms. In internal shocks, only $\lesssim$40% of the kinetic energy of the shell can be converted into radiation (Piran, 1998; Sari & Piran, 1997).

2.2.2. EXTERNAL SHOCKS

Sari & Piran (1997) suggested that the rest of the energy is emitted later, when the ejecta hits the ambient medium — the formerly ejected stellar wind or the ISM. This emission would be radiated in other wavelengths. When the shell encounters the medium, it is slowed down and an external shock emerges. A forward shock (the blast wave) continues to run into the surrounding medium, while a second reverse shock is moving backwards. When the blast wave propagates further into the medium, kinetic energy is converted into internal energy. The medium is being heated up and the accelerated electrons emit synchrotron radiation. While the shock continues, it sweeps up the medium and slows down — this results in radiation at lower wavelengths, e.g., in X–Rays, the optical and in the radio regime (Bouwhuis, 2005).

The afterglow light–curve reflects the evolution of the shock through the surrounding medium. At the beginning — in the so–called radiative phase — the energy conversion into electrons is very effective, resulting in a fast radiative cooling. After a timescale of a few days, the evolution of the jet switches from radiative to adiabatic evolution. Having swept up as much mass as the shock contained originally, the energy of the spherical shock remains constant while evolving farther into the medium (Sari et al., 1998; Preece et al., 2002).

2.3. PHOTON EMISSION

As described above, the electrons in the shock fronts are distributed according to a power–law by the Fermi shock acceleration mechanism. In the magnetic field, they emit synchrotron radiation. The synchrotron photons themselves can then interact with the primary e^- and be upscattered via inverse Compton scattering to higher energies. The electron distribution determines the emitted γ–Ray spectrum. This yields for a power–law spectral shape. A break in the energy is introduced by the effective radiative cooling of electrons with energies $E > \epsilon_\gamma$. A good parametrization of the spectrum is therefore given by a broken power–law distribution (Waxman & Bahcall, 1997). Its shape can be fully described by the two spectral indices α_γ and β_γ and the break energy ϵ_γ:

$$F_\gamma(E_\gamma) = \frac{\mathrm{d}N(E_\gamma)}{\mathrm{d}E_\gamma} = f_\gamma \cdot \begin{cases} \left(\frac{\epsilon_\gamma}{\mathrm{MeV}}\right)^{\alpha_\gamma} \left(\frac{E_\gamma}{\mathrm{MeV}}\right)^{-\alpha_\gamma} & \text{for } E_\gamma < \epsilon_\gamma \\ \left(\frac{\epsilon_\gamma}{\mathrm{MeV}}\right)^{\beta_\gamma} \left(\frac{E_\gamma}{\mathrm{MeV}}\right)^{-\beta_\gamma} & \text{for } E_\gamma > \epsilon_\gamma \end{cases} \tag{2.1}$$

The normalization f_γ is fixed by the total measured fluence, i.e., the integral over the spectrum the measured energy range:

$$\mathcal{F}_\gamma = \int \mathrm{d}E_\gamma F_\gamma(E_\gamma) \tag{2.2}$$

2.4. NEUTRINO EMISSION

In the internal shocks of the relativistic outflow, p^+ are assumed to be accelerated among with the e^- up to energies $\gtrsim 10^{20}\,\mathrm{eV}$. It is usually assumed that the fireball energy is dissipated equally into electrons and protons (Waxman & Bahcall, 1997; Waxman, 2000; Guetta et al., 2004). The high energy electrons emit synchrotron radiation that leads to the observed MeV photons of the prompt burst emission. The high energetic protons from Gamma Ray Bursts could explain the spectrum of Cosmic Rays at ultra high energies (UHECR), if the efficiency to accelerate p^+ was similar to the e^- acceleration efficiency (Dermer & Razzaque, 2010). The accelerated protons can interact with the synchrotron photons emitted by the e^-, as well as scatter with other protons or neutrons present in the shock. These interactions produce pions. The decay of the neutral pion produces a photon signal, whereas the charged pions give rise to a neutrino signal.

$$\begin{aligned} \pi^0 &\longrightarrow \gamma + \gamma \\ \pi^+ &\longrightarrow \mu^+ + \nu_\mu \longrightarrow e^+ + \nu_e + \overline{\nu}_\mu + \nu_\mu \\ \pi^- &\longrightarrow \mu^- + \overline{\nu}_\mu \longrightarrow e^- + \overline{\nu}_e + \nu_\mu + \overline{\nu}_\mu \end{aligned} \tag{2.3}$$

The photons can only escape the emitting region as soon as the shock has become optically thin. Neutrinos, on the other hand, can escape even the densest regions due to their very small cross section.

If, for instance, internal shocks in the jet produce γ's and ν's when the jet is still inside the star (substellar jet), the photon radiation would not yet be visible, as the photons could not escape the stellar envelope. The neutrinos, on the other hand, could already leave the dense region and produce a precursor neutrino signal $10 \ldots 100\,\mathrm{s}$ before the γ–Ray signal (Razzaque et al., 2003). Similarly, a neutrino afterglow signal could emerge when the reverse shock travels back into the star and re–accelerates e^- (Waxman & Bahcall, 2000). So, in principle, certain models for Gamma Ray Bursts could be tested for by observing GRB neutrinos and their temporal deviation with respect to the prompt electromagnetic signal.

In this work, I will focus only on the expected high energy neutrino radiation in coincidence with the prompt GRB signal.

2.4.1. THE PROMPT NEUTRINO SIGNAL

Waxman & Bahcall (1997) were the first to derive neutrino spectra for Gamma Ray Bursts. I will follow their argumentation in the following. They showed that protons of $\sim 10^{15}\,\mathrm{eV}$ interact with $\sim 1\,\mathrm{MeV}$ photons to produce a burst of $\sim 10^{14}\,\mathrm{eV}$ neutrinos via photo–meson production

$$p^+ + \gamma \Longrightarrow \pi^+ \longrightarrow \mu^+ + \nu_\mu \longrightarrow e^+ + \nu_e + \overline{\nu}_\mu + \nu_\mu \tag{2.4}$$

The high photon density in the outflow yields a high interaction rate of this process (Waxman & Bahcall, 1997). The large amount of produced pions should lead to a strong high energy neutrino signal in coincidence with the prompt γ emission.

The shape of the neutrino spectrum is determined by the proton and the photon spectra (see eq. 2.1). Due to the Fermi shock acceleration mechanism, the protons are power–law distributed. The interaction of the protons with the photons results in a broken power–law neutrino spectrum, which, at lower energies, follows the photon spectrum.

The pions produced in (2.4) would carry $\sim 20\%$ of the initial proton energy, leading to neutrinos with $\sim 0.05 E_p$. Consequently, neutrinos above 5% of the proton energy essentially trace the proton spectrum. A break in the spectrum is introduced by the threshold energy (in the source's rest–frame) to produce the Δ–resonance. Above this energy, a significant amount of energy of the accelerated protons would be lost due to pion production (Waxman & Bahcall, 1997). Below this break, the spectrum is harder by one power of energy. A second break ϵ_2 in the spectrum is due to efficient synchrotron cooling of high energy μ and π before they can decay into neutrinos (see, e.g., Abbasi et al., 2010).

The neutrino prompt spectrum is thus given by

$$F_\nu(E_\nu) = \frac{\mathrm{d}N(E_\nu)}{\mathrm{d}E_\nu} = f_\nu \cdot \begin{cases} \left(\frac{\epsilon_1}{\mathrm{GeV}}\right)^{\alpha_\nu} \left(\frac{E_\nu}{\mathrm{GeV}}\right)^{-\alpha_\nu} & \text{for } E_\nu < \epsilon_1 \\ \left(\frac{\epsilon_1}{\mathrm{GeV}}\right)^{\beta_\nu} \left(\frac{E_\nu}{\mathrm{GeV}}\right)^{-\beta_\nu} & \text{for } \epsilon_1 < E_\nu < \epsilon_{\nu,2} \\ \left(\frac{\epsilon_1}{\mathrm{GeV}}\right)^{\beta_\nu} \left(\frac{\epsilon_2}{\mathrm{GeV}}\right)^{\gamma_\nu - \beta_\nu} \left(\frac{E_\nu}{\mathrm{GeV}}\right)^{-\gamma_\nu} & \text{for } \epsilon_{\nu,2} \leq E_\nu \end{cases} \tag{2.5}$$

with the break energies

$$\epsilon_1 = 5 \cdot 10^5\,\mathrm{GeV} \frac{1}{(1+z)^2} \left(\frac{\Gamma_{\mathrm{jet}}}{10^{2.5}}\right)^2 \left(\frac{\mathrm{MeV}}{\epsilon_\gamma}\right) \tag{2.6}$$

$$\epsilon_2 = 10^7\,\mathrm{GeV} \frac{1}{1+z} \sqrt{\frac{\epsilon_e}{\epsilon_B}} \left(\frac{\Gamma_{\mathrm{jet}}}{10^{2.5}}\right)^4 \left(\frac{t_{\mathrm{var}}}{0.01\,\mathrm{s}}\right) \sqrt{\frac{10^{52}\,\mathrm{erg/\,s}}{L_\gamma^{\mathrm{iso}}}} \tag{2.7}$$

and the energy exponents from the photon indices:

$$\alpha_\nu = 3 - \beta_\gamma\ ,\ \beta_\nu = 3 - \alpha_\gamma\ ,\ \gamma_\nu = \beta_\nu + 2 \tag{2.8}$$

The normalization depends on the photon spectrum normalization as well as on the overall fraction of the proton energy transformed into pions. In a single interaction, in average $\langle x_{p\to\pi} \rangle = 20\%$ of the proton energy is transferred to the pion. To estimate the overall energy conversion, Abbasi et al. (2010) introduced the expression $1 - (1 - \langle x_{p\to\pi} \rangle)^{\Delta R/\lambda_{p\gamma}}$ with ΔR being the size of the shock and the mean free path of a proton for photo–meson interactions, $\lambda_{p\gamma}$. Their ratio is given by

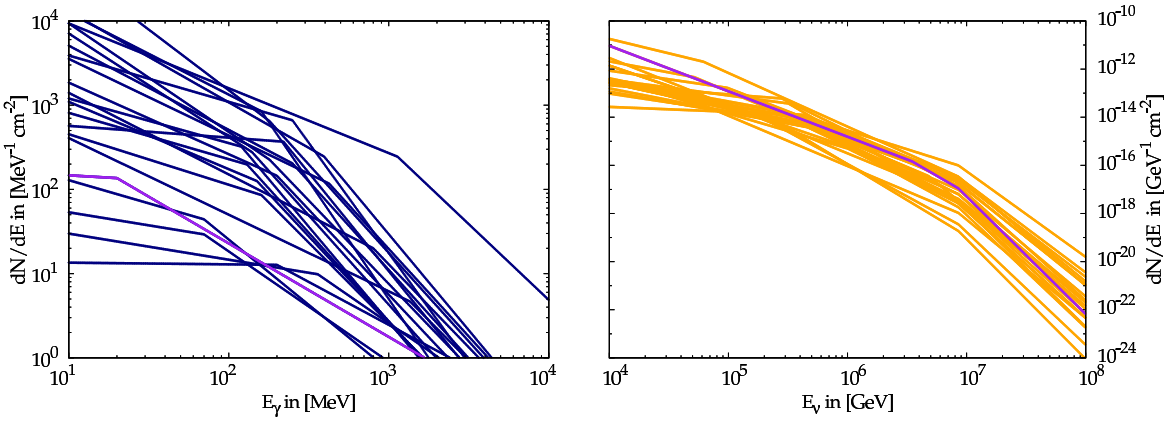

Figure 2.3.: The calculated γ spectra for the selected bursts on the left hand side. The right hand panel shows the respective neutrino spectra. The burst GRB080218B is highlighted in purple.

$$\frac{\Delta R}{\lambda_{p\gamma}} = \left(\frac{L_\gamma^{\mathrm{iso}}}{10^{52}\,\mathrm{erg/\,s}}\right)\left(\frac{0.01\,\mathrm{s}}{t_{\mathrm{var}}}\right)\left(\frac{10^{2.5}}{\Gamma_{\mathrm{jet}}}\right)^4\left(\frac{\mathrm{MeV}}{\epsilon_\gamma}\right). \tag{2.9}$$

Thus the neutrino spectrum normalization can be calculated via

$$\int_0^\infty \mathrm{d}E_\nu F_\nu(E_\nu) = \frac{1}{8}\frac{1}{f_e}\left(1-(1-\langle x_{p\to\pi}\rangle)^{\Delta R/\lambda_{p\gamma}}\right)\cdot\mathcal{F}_\gamma \tag{2.10}$$

with the known γ–ray fluence $\mathcal{F}_\gamma$ from the integral (2.2) over the energy range measured by the detector. In these equations, z is the cosmological redshift, ϵ_e and ϵ_B are the fractions of jet energy in electrons and the magnetic field, respectively. Following Becker (2008), the ratio f_e of the jet energy in electrons and protons is set to 0.1. L_γ^{iso} is the isotropic luminosity of the burst, t_{var} is its variability from the light curve and Γ_{jet} is the Lorentz boost factor. Figure 2.3 shows the calculated photon spectra and neutrino spectra for a set of selected bursts.

The discovery of neutrinos from Gamma Ray Bursts would corroborate the fireball scenario and give proof to the proton acceleration assumption. This could help establishing GRBs as possible UHECR sources. Furthermore, by testing the simultaneity of the GRB photons and neutrinos, the special relativity assumption on the limiting speed of particles could be investigated. This could also test for the weak equivalence principle, by determining the time delay as photons and neutrinos pass through the same gravitational potential (Waxman & Bahcall, 1997).

3. ANALYSIS

3.1. GAMMA RAY BURST SELECTION

The first step in the analysis chain was to preselect a set of suitable Gamma Ray Bursts for an analysis with the ANTARES neutrino detector. Apart from the actual GRB parameters, it is also important that it occurred in the respective field of view of ANTARES, i.e., under the horizon. The data taking conditions of the detector at the GRB time were taken into account, too. Only the bursts with the highest expected neutrino fluxes, which occurred at data taking runs of the detector with low background rate, have been selected.

To perform this selection, the program GRBSAMPLE was implemented. It reads in a complete table of ANTARES data taking runs, compiled by Friederike Schöck. This table contains all important run information such as its start and stop time, the meanrate of the optical background, the mean sea current velocity, the respective set of running triggers etc. The runs usually contain approximately 3 h of data, but the actual duration is depending on the amount of data taken. All parameters from the table are stored internally in a list of runs.

The Gamma Ray Burst information is taken from a table by Alexander Kappes, who collected the information published by the GCN network (see UK Swift Science Data Centre, 2010) on each burst. In order to check whether the burst occurred under the ANTARES horizon, the bursts' coordinates given in right ascension and declination are converted into local coordinates Zenith and Azimuth, as shown in fig. 1.7. Only the bursts producing upgoing signal in the detector were selected. The time of the burst was compared to the start and stop times in the run list to find the respective data taking run, in which the burst occurred. If the could be found and the optical background meanrate of that time was lower than 100 kHz, the burst was stored in a list, containing all bursts which occurred at acceptably ANTARES data taking conditions and were in principle visible for the detector.

We only want to focus on the bursts which are expected to produce the strongest neutrino signals. For this reason, the photon spectrum of each GRB is calculated from the respective set of spectral parameters, as measured by the GCN network (UK Swift Science Data Centre, 2010). From this information, the neutrino spectrum (as given in equations (2.1), (2.2) and (2.5)) can be derived. The neutrino spectrum is integrated above 1 TeV to find the bursts from which the highest neutrino fluxes would be expected. The strongest bursts with a resulting neutrino flux $> 10^{-8}\,\mathrm{cm}^{-2}$ were considered candidates for further investigation. Around twenty bursts were found in between the years 2007 to 2009.

In principle, the following analysis is applicable to all bursts, but in this work I focused exemplary on the burst GRB080218B.

3.1.1. THE BURST GRB080218B

The burst GRB080218B was detected by the *Swift* satellite on February 18, 2008 at 23:57:47 UT (Schady, 2008). *Swift* located the burst with an accuracy of $\sim 3'$ at a right ascension

of 177.96° and a declination of −53.1° (Schady et al., 2008). In its quite short duration of $T_{90} = 6.2\,\mathrm{s}$ a fluence of $5.1 \cdot 10^{-7}\,\mathrm{erg/\,s}$ was detected in the $15 \ldots 150\,\mathrm{keV}$ band. The redshift was determined to be $z < 3.3$. Converted into local coordinates of the ANTARES detector, it occurred at a Zenith angle of 98.11° and an Azimuth of 282.39°. The respective ANTARES data taking run number is 32165. It started at 21:48 local time at the site and ended the next day, February 19 at 00:58 after about 3 hours of data taking. At this time, lines 11 and 12 were out of order. The optical background was quite low with a meanrate of 62.39 kHz. According to the *Waxman–Bahcall*–spectrum (eq. 2.5), a neutrino flux of $8.11 \cdot 10^{-7}\,\mathrm{cm}^{-2}$ above 1 TeV would be expected at the Earth from this GRB — one of the highest in the preselected sample. The spectral indices which determine the photon and neutrino spectra (see eq. 2.1 and 2.5) are

photon spectrum	neutrino spectrum
$f_\gamma = 1.36 \cdot 10^2\,\mathrm{MeV}^{-1}\,\mathrm{cm}^{-2}$	$f_\nu = 1.45 \cdot 10^{-16}\,\mathrm{GeV}^{-1}\,\mathrm{cm}^{-2}$
$\epsilon_\gamma = 0.02\,\mathrm{MeV}$	$\epsilon_1 = 3.50\,\mathrm{PeV}$
	$\epsilon_2 = 8.54\,\mathrm{PeV}$
$\alpha_\gamma = 0.11$	$\alpha_\nu = 1.89$
$\beta_\gamma = 1.11$	$\beta_\nu = 2.89$
	$\gamma_\nu = 4.89$

3.2. PREPARATION OF THE DATA

3.2.1. CUTTING OF EVENTS

The program ADDWEIGHTS reads in the Monte Carlo simulated files and adjusts them for the following GRB analysis. Each event in these files has a certain primary particle direction. As the sample simulates atmospheric neutrinos, it contains events equally spread all over the sky. We want to reduce this to a region of interest around the actual Gamma Ray Burst direction. For this, all events within a certain search cone are cut out. The program reads in the MC sample and calculates the angle between the GRB coordinates (in Zenith and Azimuth) and the Monte Carlo simulated particle for each frame. Only if this angle was $\leq 5°$, the frame was kept. With this procedure, a new Monte Carlo sample with $\sim$3000 events is sorted out. Figure 3.1 shows a sky map of the selected events.

3.2.2. WEIGHTING

In order to estimate the flux as it can be detected by ANTARES, not only the expected neutrino flux from eq. (2.5), but also the detector's sensibility has to be taken into account. For this purpose, three weighting parameters have been introduced in the ANTARES Monte Carlo simulations (see Brunner, 1999; Kappes & Katz, 2005) : The weight $w1$ represents the angular dependent effective can surface of ANTARES $A(E, \Theta, \xi)$. The normalization factor or so-called generation weight $w2$ contains the sampling area $w1$, angular and energy phase space factors, the total energy dependent neutrino cross section $\sigma(E)$, the number of target nucleons per m^3 and the probability for a neutrino to penetrate the Earth. It has the unit

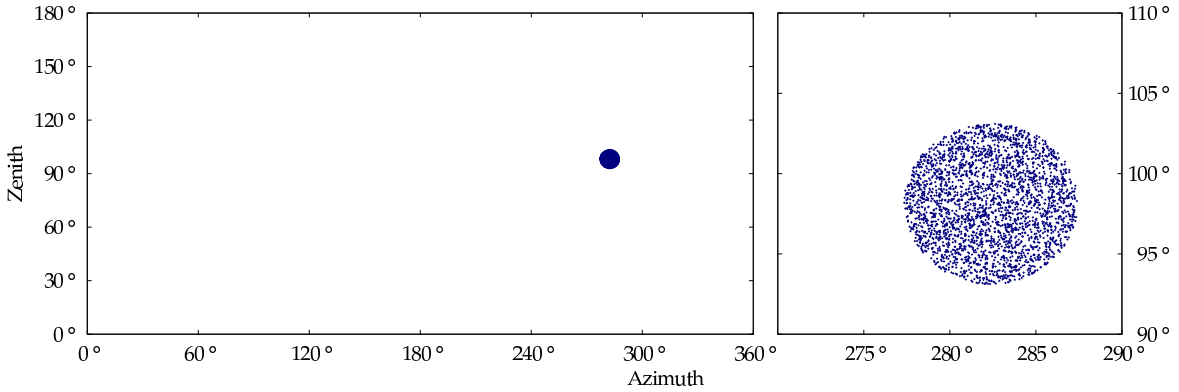

Figure 3.1.: A sky map of the selected Monte Carlo events within a cone of 5° around the burst position. Azimuth and Zenith are the local coordinates of the ANTARES *detector.*

$[\,\mathrm{GeV\,m^2\,sr}]$. It describes the sensibility of ANTARES to detect a neutrino with a certain energy E, coming from a specific direction. The global weight $w3$ then introduces the expected neutrino flux. It is the product

$$w3 = w2 \cdot \Phi \tag{3.1}$$

of the differential neutrino flux, Φ, before penetrating the Earth. The weights $w3$ which are already contained in the Monte Carlo files correspond to the atmospheric neutrino flux. They are used to estimate the background. Consequently, in the following I will call this weights w_{atm}. The very same Monte Carlo files are being used to estimate the Gamma Ray Burst neutrino signal in the ANTARES detector. No further simulations were needed as the adjustment of the event weights is sufficient to represent the signal flux. To calculate the physical flux Φ_{signal} of the burst, the spectrum $\frac{\mathrm{d}N(E_\nu)}{\mathrm{d}E_\nu}$ from eq. (2.5) has to be divided by the respective solid angle Ω of the angular search cone and the duration of the burst, T_{90}:

$$\Phi_{\mathrm{signal}} = \frac{\mathrm{d}N(E_\nu)}{\mathrm{d}E_\nu} \cdot \frac{1}{T_{90} \cdot \Omega} \tag{3.2}$$

Ω is related to the angle of the search cone ϕ via

$$\Omega = 2\pi(1 - \cos(\phi/2), \tag{3.3}$$

which yields $\Omega = 0.0239\,\mathrm{sr}$ for an opening angle of $\phi = 10°$. The signal weight for the neutrino GRB flux w_{signal} is then given by

$$\begin{aligned} w_{\mathrm{signal}} = w2 \cdot \Phi_{\mathrm{signal}} = w2 \cdot \frac{\mathrm{d}N(E_\nu)}{\mathrm{d}E_\nu} \cdot \frac{1}{T_{90} \cdot \Omega} \\ \text{in } [\,\mathrm{GeV\,cm^2\,sr}] \cdot \frac{1}{[\,\mathrm{GeV\,cm^2}]} \cdot \frac{1}{[\,\mathrm{s\,sr}]} = [1/\,\mathrm{s}] \end{aligned} \tag{3.4}$$

The two weights w_{atm} and the calculated signal weight w_{signal} are then both stored within the event file. That is, each frame ends up with two weights and can be considered as

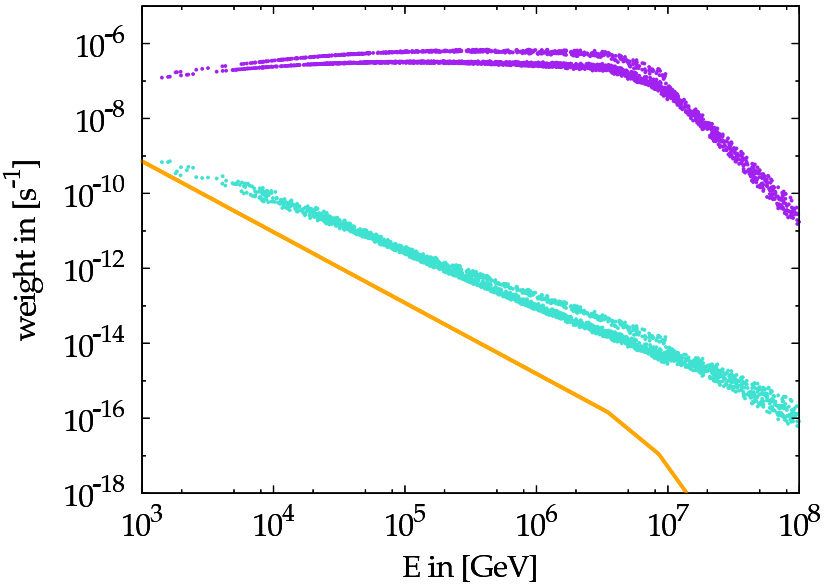

Figure 3.2: The atmospheric weights w_{atm} in turquoise and the signal weights w_{signal} in violet. The underlying spectrum for the weighting is drawn in orange.

background or signal event, depending on which of the two weights is being used for further calculations[1]. Both weights are shown in fig. 3.2, along with the neutrino signal flux in orange.

3.2.3. ADDING OF MINIMUM BIAS DATA AND CALIBRATION

In the next step, real optical background event files of the respective run are read in and added to the Monte Carlo frames. Afterwards, the data file is being calibrated according to the detector conditions of that run. Both steps are performed by the program GRBCALIB.

The REALBKGADDER–module, implemented by Holger Motz, reads in minimum bias files containing the optical background events. These are stored as maps of pulses detected in the Optical Modules. When processing the data set, for each Monte Carlo frame an event of the minimum bias files is chosen randomly and the respective pulses are added to the MC frame. Furthermore, the conditions of the OMs are excerpted and later on used to calibrate the full data set. This information is stored within each minimum bias frame as *OMConditionMap*. Employing this technique, the conditions at the actual data taking time are simulated as realistic as possible. The program also communicates with the ANTARES database and queries the set of triggers, which were operating during the data taking run. Subsequently, the whole file is calibrated applying the OM conditions and the respective trigger setup of the run.

3.2.4. RECONSTRUCTION: AART'S STRATEGY

The reconstruction of the event files is performed with the AART STRATEGY (Heijboer, 2004), which is also implemented in the SEATRAY–framework. Using the pulses in the optical modules, this algorithm tries to find particle tracks which could give rise to the detected

[1]Note that the expected flux is simply calculated by summing up over the event weights, as will be explained later in section 3.2.5.

Čerenkov photon hits. More precisely, the probability density function of hit times is optimized using a maximum likelihood fit (see, however, Heijboer, 2004, for further description of the algorithm.).

After the fit, a reconstruction quality parameter Λ is assigned to each track. It describes how well the algorithm could fit its direction. Heijboer (2004) could show that for reasonable cuts, the method yields angular resolutions of typically less than $\sim 0.2^\circ$. Consequently, for energies below 10 TeV, the resolution is dominated by the scattering angle $\langle \Theta_S \rangle$ between primary neutrino and muon (see section 1.2) rather than by the angular error of the reconstruction. As already mentioned above, most of the atmospheric muon background can efficiently be reduced by selecting only upgoing reconstructed tracks ($\Theta > 90^\circ$). Yet still, there do remain falsely reconstructed atmospheric muons as well as the irreducible background from atmospheric neutrinos (~ 10 events per day). A cut on the quality parameter $\Lambda > -5.3$ could be proven to reduce the atmospheric muon flux by a factor of 10^5 to a remainder of around one event per day (see Heijboer, 2004, p. 81).

3.2.5. CUTS

After the reconstruction of the Monte Carlo event files, the ratio of the expected signal and background fluxes can be influenced by certain selection parameters. As mentioned above, cutting on the Zenith angle Θ or the reconstruction quality parameter Λ, e.g., suppress background events efficiently. Due to the short duration of GRBs and their accurately defined sky positions, the background is already very low. The Zenith angle selection has already been taken care of by preselecting only bursts occurring below the ANTARES horizon. Further selection parameters are investigated in the following. The criteria are optimized such, that when applying them to actual data (the unblinding process), the analysis would yield for preferably significant discoveries.

The expected number of background and signal events is calculated by summing up the event weights and multiplying by the burst's duration:

$$\mu_\mathrm{b} = \sum_i w^i_\mathrm{atm} \cdot T_{90} \qquad\qquad \mu_\mathrm{s} = \sum_i w^i_\mathrm{signal} \cdot T_{90} \tag{3.5}$$

If further cuts are applied, only the events in accordance with the chosen cuts are summed up. The efficiency of a set of cut parameters is given by the ratio of number of selected events to the full sample:

$$\eta = \frac{\mu^\mathrm{cuts}}{\mu^\mathrm{all}} = \frac{\sum_\mathrm{cuts} w^i}{\sum_\mathrm{all} w^i} \tag{3.6}$$

The cuts shall be efficient in reducing the background, whereas on the other hand keeping as much signal as possible. In this work, I focussed on three parameters: The quality parameter Λ of the AART STRATEGY, the number of hits n_hits produced by the event and the opening angle Δ_max around the GRB direction.

RECONSTRUCTION QUALITY Λ

The quality parameter Λ is a measure of how well the algorithm could fit a track to a certain pattern of hits in the OMs. Tracks with low values of Λ are usually reconstructed far

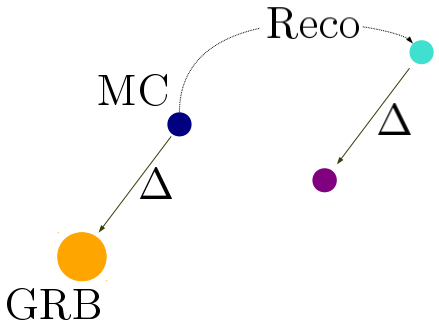

Figure 3.3: The principle of the 'shift' of events in fig. 3.4. Knowing the displacement Δ between the burst (orange) and the Monte Carlo event direction (blue), this can be used to shift the reconstructed Monte Carlo track as if it would have originated from the burst direction (violet).

away from the original track, thus a cut on this parameter selects the events where the reconstructed tracks are mostly closer to the Monte Carlo 'truth'. Consequently, by choosing a certain Λ–cut, the angular resolution of the reconstruction can be strongly increased. The parameter space was restricted to $\Lambda > -5.3$ (see section 3.2.4).

In the upper panel of fig. 3.4, the spread of the reconstructed events on the sky is shown in blue. It is striking that a lot of events are reconstructed far away from the 5° search cone (drawn in blue), from where they originated. A cut on Λ significantly improves this situation. The selected events with $\Lambda > -5.3$ are shown in turquoise. Still, some badly reconstructed events remain, but the main part of the ∼3000 events is well focussed in the search cone.

NUMBER OF TRIGGERED HITS n_{HITS}

The energy reconstruction of particles with ANTARES is very challenging. One measure of the energy is for instance the track length of a particle. But if the track exceeds the detector dimensions, its actual length cannot be determined. A cut on the particle's energy would, on the other hand, be a very powerful tool for background reduction. As shown in fig. 3.2, the Gamma Ray Burst neutrino signal strongly dominates the flux at higher energies. For energies above $\sim 10^5$ GeV, it exceeds the atmospheric neutrino flux by five orders of magnitude. Since the energy cannot be determined easily, the number of hits an event triggered in the detector n_{hits} can be used to roughly estimate its energy .

OPENING ANGLE Δ_{MAX}

When searching for Gamma Ray Burst neutrinos, it is of course reasonable to restrict the analysis to a certain angle around the burst direction. This is a powerful tool to suppress the background spread equally all over the sky. A statistical error in the reconstructed signal events is introduced, however, by the scattering angle Θ_S between the muon and the primary neutrino and the uncertainties in the angular reconstruction. So the opening angle cannot be chosen arbitrarily small without cutting signal events. But as shown above, the angular resolution of the reconstruction is — depending on the choice of cut parameters — smaller than 1° (see section 3.2.4). As shown in fig. 1.4, $\langle\Theta_S\rangle$ decreases very fast for higher energies. Above 100 GeV, it is well below 1°.

In this analysis, no neutrino signal from the actual GRB direction was simulated, but instead, a previously simulated set of Monte Carlo data is being used. Each of the MC

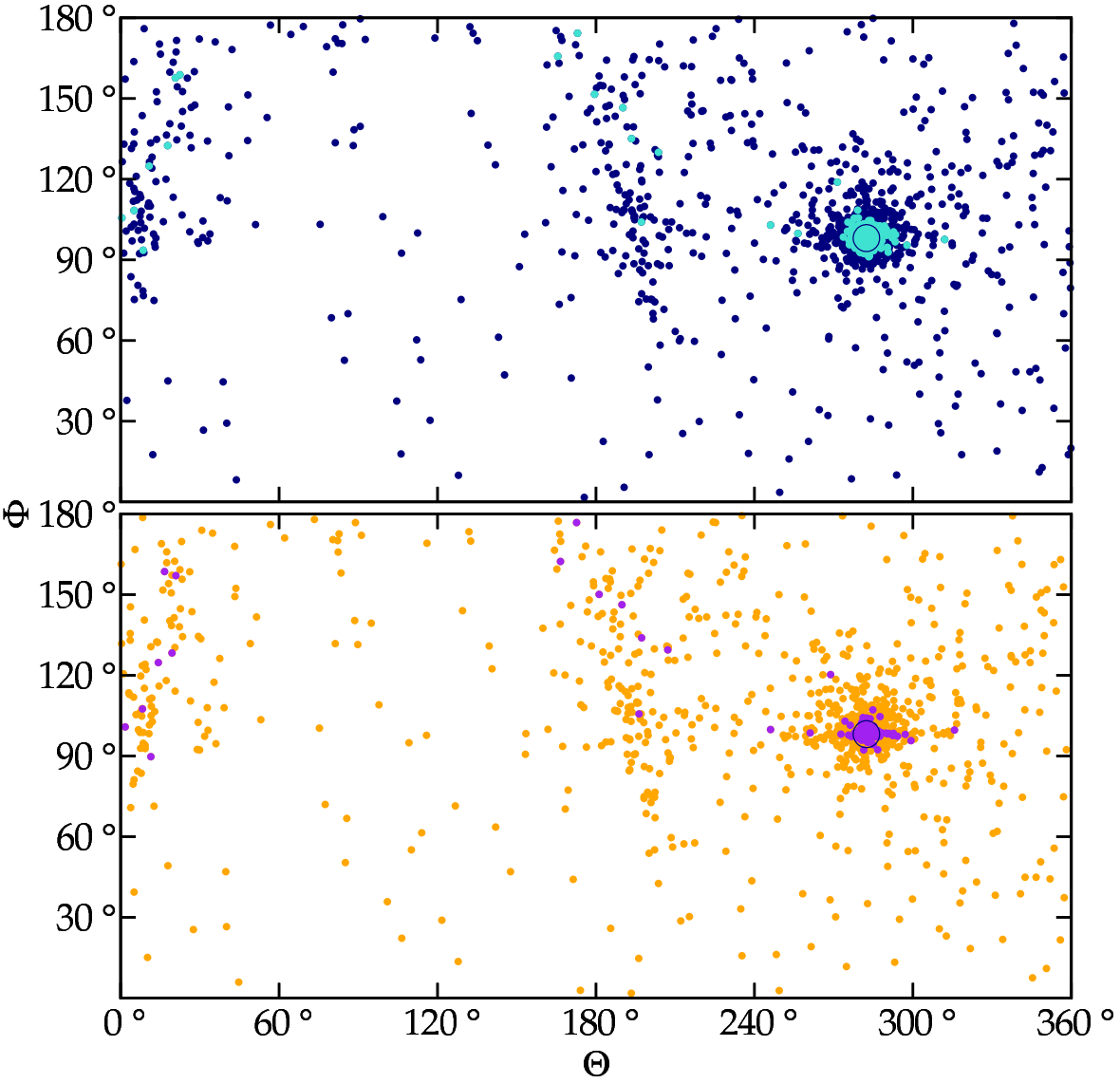

Figure 3.4.: A sky map of the Monte Carlo events as reconstructed with AART. *The events with a quality fit parameter* Λ *of* > -5.3 *are plotted in turquoise and purple. In the upper panel, the original MC reconstructed directions are plotted, whereas in below, all the event directions were shifted as if the original track would have come from the exact GRB Azimuth and Zenith. This is only possible since the 'real' MC origin within the angle cone and therefore its respective misplacement from the GRB Azimuth and Zenith angle is known. The principle is shown in fig. 3.3. The* 5° *cone, to which the MC event sample has been cut, is drawn in blue.*

events contains two weights (see section 3.2.2), which represent the atmospheric neutrino flux and the GRB neutrino flux. These events are equally distributed in the 5° cone around the burst direction. A cut on the angle between the burst direction and the reconstructed Monte Carlo track would consequently cut signal and atmospheric events similarly without improving the analysis. Nevertheless, it would be desirable to imitate the angular cut in some way. Knowing the displacement of the Monte Carlo event with respect to the Gamma Ray Burst direction Δ, one could in principle shift the reconstructed track direction by this displacement Δ (see fig. 3.3). Figure 3.4 shows how this influences the whole sky distribution. The events with $\Lambda > -5.3$ are drawn in violet. Because of the selected search cone, this difference Δ must be smaller than 5°. So we assume the displacement between the reconstructed and original tracks to be similar for tracks lying $\lesssim 5^\circ$ apart in order to roughly estimate the behaviour of signal and background events when applying an angular cut. This is of course not completely accurate and will be discussed in section 3.5. Note that the described 'shifting' was never performed to modify the data, but only for illustration in fig. 3.4.

When 'applying' the angle cut, the sums (3.5) are performed differently for the atmospheric flux μ_b and the signal flux μ_s. To estimate the atmospheric flux, the events within a certain maximal angle around the burst direction are selected. To estimate the signal flux, on the other hand, we want to treat the Monte Carlo events as if they originated from the burst direction. This can be done by mathematically shifting the directions in the way shown in fig. 3.3. But this would yield for the same result as simply cutting on the angle between the reconstructed and the initial MC track.

$$\mu_\mathrm{b} = \sum_i w^i_\mathrm{atm} \cdot T_{90} \qquad \text{where } \Delta^\mathrm{Reco}_\mathrm{GRB} < \Delta_\mathrm{max} \tag{3.7}$$

$$\mu_\mathrm{s} = \sum_i w^i_\mathrm{signal} \cdot T_{90} \qquad \text{where } \Delta^\mathrm{Reco}_\mathrm{MC} < \Delta_\mathrm{max} \tag{3.8}$$

3.3. STATISTICS

3.3.1. GENERAL STATISTICS

The neutrino events in the ANTARES detector are assumed to be Poisson distributed. This distribution describes the probability to observe a number of events n_obs in a given (time) interval, when the events occur independently of each other with a given mean rate μ (see, for example, Particle Data Group, 2008, and references therein.).

$$P(n|\mu) = e^{-\mu}\frac{\mu^n}{n!} \tag{3.9}$$

To distinguish between a real present signal and the 'background only' hypothesis, we want the probability to observe n_obs events when no signal is present (the so-called p-value)

$$P(\geq n_\mathrm{obs}|\mu_\mathrm{b}) = \alpha \tag{3.10}$$

to be very small. The p-value defines the significance level of a discovery. The smaller α, the more significant is the detection of n_{obs} or more events:

$$\begin{aligned} 5\sigma &\longrightarrow \alpha < 2.87 \cdot 10^{-7} \\ 6\sigma &\longrightarrow \alpha < 9.87 \cdot 10^{-10} \\ 7\sigma &\longrightarrow \alpha < 1.28 \cdot 10^{-12} \\ 8\sigma &\longrightarrow \alpha < 6.22 \cdot 10^{-16} \ \ldots \end{aligned} \tag{3.11}$$

The significance levels on the right–hand side of eq. (3.11) are given by the probability of a Gaussian statistic to be observed at at least $5, 6, 7 \ldots$ standard deviations from the expected mean value (Sinervo, 2002). They are defined by the respective integrals over a Gaussian's tail. So, e.g., claiming a 5–σ discovery with a single discovered event requires the probability to observe one event when only background is present to be smaller than $2.87 \cdot 10^{-7}$. Note, however, the importance of exactly determining the background in this context as the significance level only depends on the expected background rate μ_{b}.

Assuming the presence of a real signal μ_{s}, the probability to detect it is given by the so–called statistical power $(1-\beta)$:

$$1 - \beta = P(\geq n_{\mathrm{obs}} | \mu_{\mathrm{b}} + \mu_{\mathrm{s}}) \tag{3.12}$$

In Gamma Ray Burst analyses with neutrino telescopes, the number of expected events is only very small. Hence we want to optimize the analysis for the observation of a single event, i.e., $n_{\mathrm{obs}} = 1$. Since

$$P(\geq n_{\mathrm{obs}} | \mu) = \sum_{n=n_{\mathrm{obs}}}^{\infty} P(n|\mu) = 1 - \sum_{n=0}^{n_{\mathrm{obs}}-1} P(n|\mu) = 1 - P(< n_{\mathrm{obs}} | \mu), \tag{3.13}$$

the equations (3.10) and (3.12) reduce to

$$\alpha = P(\geq 1 | \mu_{\mathrm{b}}) = 1 - P(0|\mu_{\mathrm{b}}) = 1 - e^{-\mu_{\mathrm{b}}} \tag{3.14}$$

$$1 - \beta = P(\geq 1 | \mu_{\mathrm{b}} + \mu_{\mathrm{s}}) = 1 - P(0|\mu_{\mathrm{b}} + \mu_{\mathrm{s}}) = 1 - e^{-(\mu_{\mathrm{b}} + \mu_{\mathrm{s}})} \tag{3.15}$$

3.3.2. MODEL DISCOVERY POTENTIAL

In high energy physics, a commonly used tool to optimize an analysis for discovery is the *Model Discovery Potential* MDP. In the following, I will show how it is calculated for a given set of expected background μ_{b} and signal events μ_{s} (see, e.g., Hill et al., 2006).

For a given significance level α, the critical number n_{crit} can be calculated: it is the smallest number of observed events needed to report a detection of the desired significance. It is evaluated by inverting eq. (3.10) for a chosen p-value (see the inequalities eq. 3.11). With increasing background rates, the probability to detect background events would also rise. That means, for higher backgrounds, more than one observed events might be necessary in order to yield for a significant signal detection ($n_{\mathrm{crit}} > 1$).

If we want to observe $\geq n_{\mathrm{crit}}$ events with a specified probability $(1-\beta)$, this requires a certain signal strength, the so–called *least detectable signal*. This is the necessary signal to yield a fixed statistical power $(1-\beta)$ at a certain significance level. For given values of α

and $(1-\beta)$, the least detectable signal μ_{lds} only depends on the expected background μ_{b}.[2] A commonly used choice is to fix the significance to 5 σ (i.e., $\alpha = 2.87 \cdot 10^{-7}$ according to eq. 3.11) and the statistical power at $(1-\beta) = 90\%$. These values were also chosen in this work.

The ratio of the required signal and the actual expected signal is called *Model Discovery Potential*:

$$MDP = \frac{\mu_{\text{lds}}}{\mu_{\text{s}}} \tag{3.16}$$

If the actual signal μ_{s} was as strong as the least detectable signal, it would as well be detected with a probability of $(1-\beta)$ with a significance of α. In this case, the Model Discovery Potential would equal one. If, on the other hand, the signal was much weaker than that, the significance of a detection would still be the same, but the detection would be much less probable. In this case, the ratio would be larger, $MDP > 1$. Values below one would be most favourable, as they imply the signal being even stronger than the least detectable signal, i.e., it would be detected with an even larger probability than $(1-\beta)$. Thus the MDP describes a kind of 'scaling factor', which represents, by how much a signal is too strong or faint to be detected with exactly $(1-\beta)$ probability at a certain significance level. An optimization of an analysis would always aim at minimizing the Model Discovery Potential.

3.4. RESULTS

This work focussed on three cut parameters, the quality of the reconstruction Λ, the number of hits n_{hits} and the opening angle Δ_{max}. By exploiting the *Model Discovery Potential* method, I intended to optimize the analysis method.

3.4.1. MDP

Because of the low background, it was possible to fulfil the inequality in eq. (3.11) at a significance level of 5 σ for a single event, $n_{\text{crit}} = 1$. Figures 3.5 and 3.6 show the dependencies of the *Model Discovery Potential* on the cut parameters. Two things are striking: First, the MDP is in the order of $\gtrsim 2000$, a very high value. This is due to a very low probability to detect the signal. Second, its value decreases when easing the cuts onΔ_{max} and the n_{hits}, i.e., widening the angular cone or decreasing the number of required triggered hits. The reason becomes clear when looking at the pure probabilities to observe ≥ 1 event, α and $(1-\beta)$.

In fig. 3.7, the probability α to yield an event from only background is plotted in blue, whereas $(1-\beta)$, the probability to observe more than 1 event when also real signal is present, is plotted in orange. The probability $(1-\beta)$ to detect a neutrino even if a real signal is present is very low and always smaller than 0.25%. This explains the very high values of the MDP: A much stronger signal would be needed in order to detect an event with 90% probability. Obviously, the p-value is always smaller than 10^{-7} which results in

[2] Note that μ_{lds} for a given power $(1-\beta)$ is also the standard Neyman upper limit with confidence level $1-\beta$, if exactly $n_{\text{crit}} - 1$ events were reported (Hill et al., 2006).

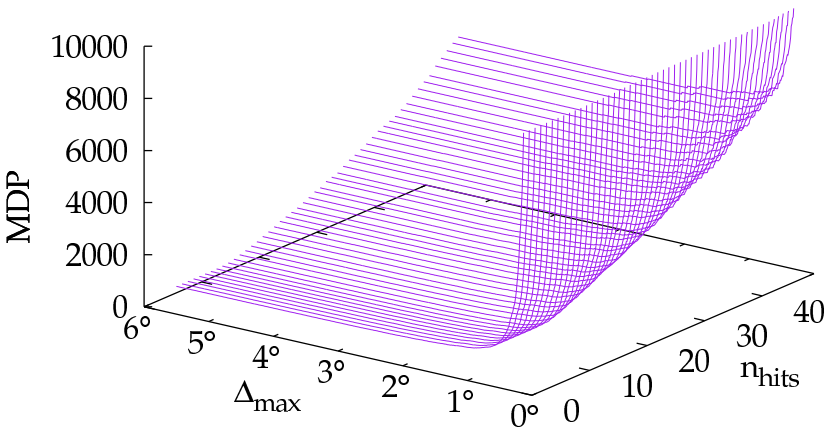

Figure 3.5: The Model Discovery Potential versus the cut parameters number of triggered hits n_{hits} and the opening angle Δ_{max}. The quality parameter cut was fixed to $\Lambda > -5.3$. The MDP decreases with looser cuts, i.e. when the opening angle becomes larger and the minimum number of hits decreases.

significances better than 5 σ (see eq. 3.11) for all choices of the cut parameters. Hence, every detection of a neutrino event would be a discovery of at least 5 σ, because the background is *a priory* so small. Since the MDP–analysis 'searches' for a significance of *exactly* 5 σ (a p-value $\alpha = 2.87 \cdot 10^{-7}$), it prefers the looser cuts which yield for more background signal. But this *worsens* the significance of a possible detection instead of increasing it. Note, however, that requiring a higher significance, e.g., 6 σ, would yield even higher values of the MDP as it requires a p-value smaller than 10^{-9}, which cannot be fulfilled.

It is hard to believe, that for instance the wider opening angles would improve the analysis method. On the contrary, a look at the probabilities already revealed, that the significance decreases with easing the cuts. In cases like this, where the expected background rate is very low, the optimization of the *Model Discovery Potential* would not yield the best set of cut parameters.

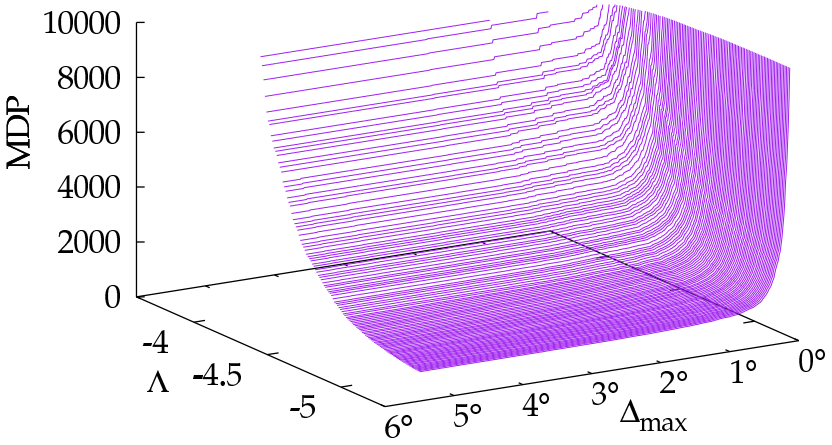

Figure 3.6: The Model Discovery Potential versus the cut parameters Λ and the opening angle. The number of triggered hits was not constrained for this plot ($n_{hits} = 0$).

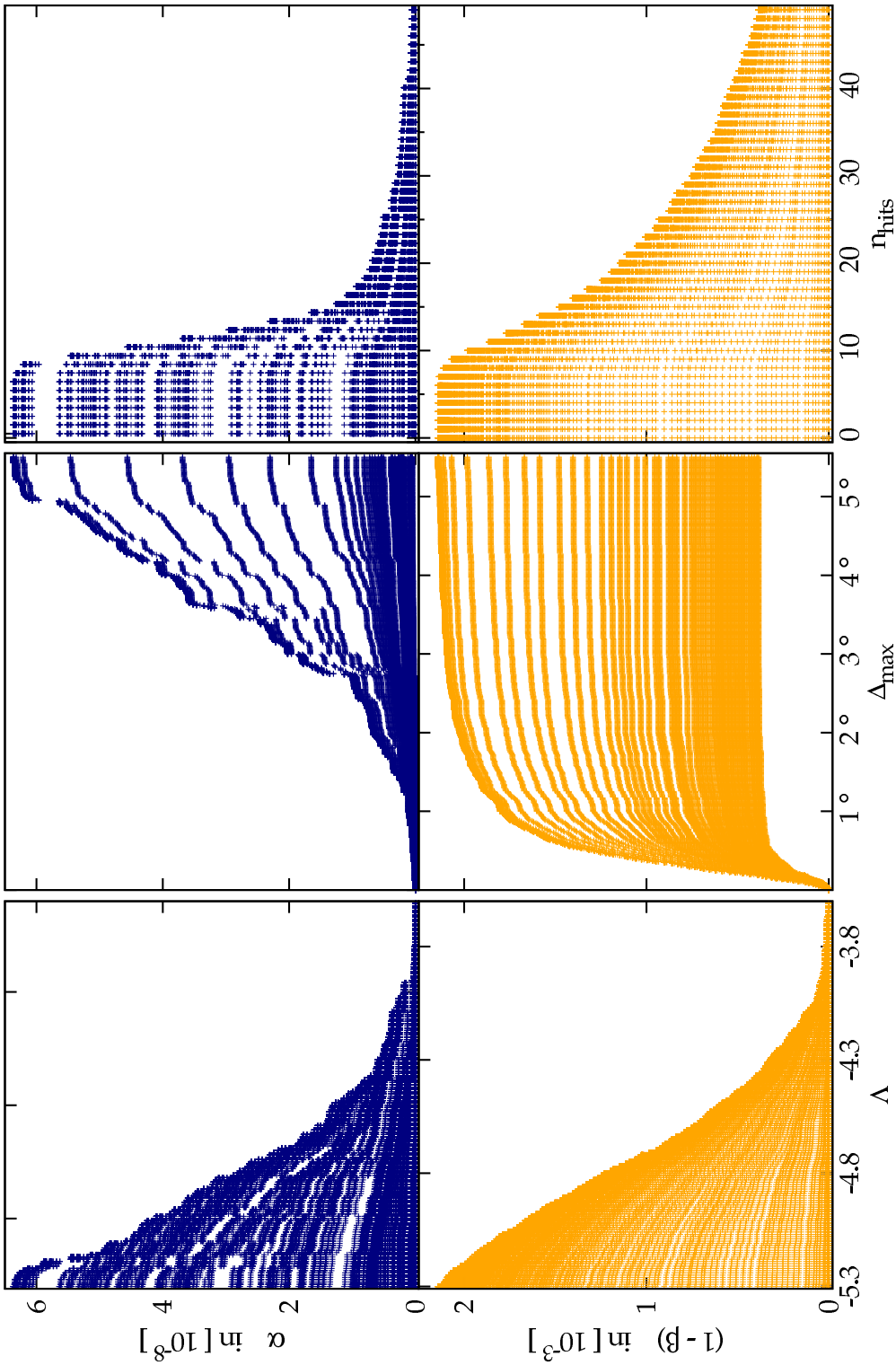

Figure 3.7.: The probabilities $\alpha = P(\geq 1|\mu_b)$ in blue and $(1-\beta) = P(\geq 1|\mu_b + \mu_s)$ in orange. These figures are the two–dimensional projections of figures A.1 and A.2 in the appendix. For each plot, two cut parameters were scanned whereas the third was fixed. The dependencies on varying the cut on the Λ parameter is shown in the two left–hand panels. Here, the number of triggered hits was not constrained. In the four right–hand panels, the dependencies of the probabilities on the opening angle and n_{hits} are shown. For these four figures, the quality parameter was fixed to $\Lambda > -5.3$.

3.4.2. CUT PARAMETERS

Instead of exploiting the Model Discovery technique, one can optimize the two probabilities α to observe events from only background and $(1-\beta)$, the probability to detect signal events. The optimal choice of cuts would yield low values for α, which improves the significance of a detection, and at the same time preferably high statistical power $(1-\beta)$.

In fig. 3.7, the dependencies of the significance level (in orange) and the statistical power (in blue) on the cut parameters are shown (note, however, figures A.1 and A.2 in the appendix). α decreases with smaller opening angles, tighter cuts on the quality parameter and increasing number of required triggered hits, as we would expect: The cuts suppress background events, which makes the detection of an event from only background more unlikely. The statistical power also decreases with stricter cuts, but the dependency is not the same as for α. Especially when looking at the angular cone, the differences in the behaviours of the two probabilities are striking. In the following, I will describe how these differences can be used to optimize the set of cut parameters.

RECONSTRUCTION QUALITY Λ The dependency of α and $(1-\beta)$ on the quality parameter of the reconstruction is drawn in the lower panels of fig. 3.7. Both decrease with stricter cuts on Λ, but the dependencies are very similar. Consequently, background as well as signal flux would be reduced likewise. Hence, it is reasonable to cut Λ at the reported value of -5.3, which was found to efficiently suppress the atmospheric muon background by Heijboer (2004).

OPENING ANGLE Δ_{MAX} We would expect a signal spread equally on the sky — like the atmospheric neutrino background — to be proportional to the squared angular cone, as it determines the area on the sky. For this reason, the opening angle is a very efficient cut parameter when searching for a signal from a point source on the sky. For a maximum wide angular cone and no cut on the number of hits, the p–value is $\alpha = 6.4 \cdot 10^{-8}$. For $\Delta_{\mathrm{max}} \leq 3^\circ$, the dependency becomes more flat with values of $\alpha \lesssim 2 \cdot 10^{-8}$. At the same time, the statistical power decreases with smaller opening angle, but at an angle of $\gtrsim 2.5^\circ$ virtually all signal events are within the cone — i.e., the probability to detect an event does not rise significantly when choosing wider search cones. This is what would be expected for a signal coming from a certain direction. Hence, an angular cut at around 2.5° would on the one hand yield for relatively high probability to detect a signal neutrino while on the other hand keeping the probability for events from background only very low at $\lesssim 2 \cdot 10^{-8}$. This yields for significances better than $5\,\sigma$.

TRIGGERED HITS n_{HITS} Note that the number of hits roughly serves as an energy estimator of the events, as more energetic particles are able to produce more Čerenkov photons in the detector. The potential power of an energy cut was already apparent when looking at the weights of the background and signal events, shown in fig. 3.2. As the GRB neutrinos are expected to have much higher energies as the atmospheric neutrinos, a cut on the energy would always highly suppress the background. When increasing the number of required triggered hits, α decreases rapidly between around 10 to 15 hits, where the function gets flatter again, yielding for quite good α–values of $\lesssim 10^{-8}$. Thus, α can

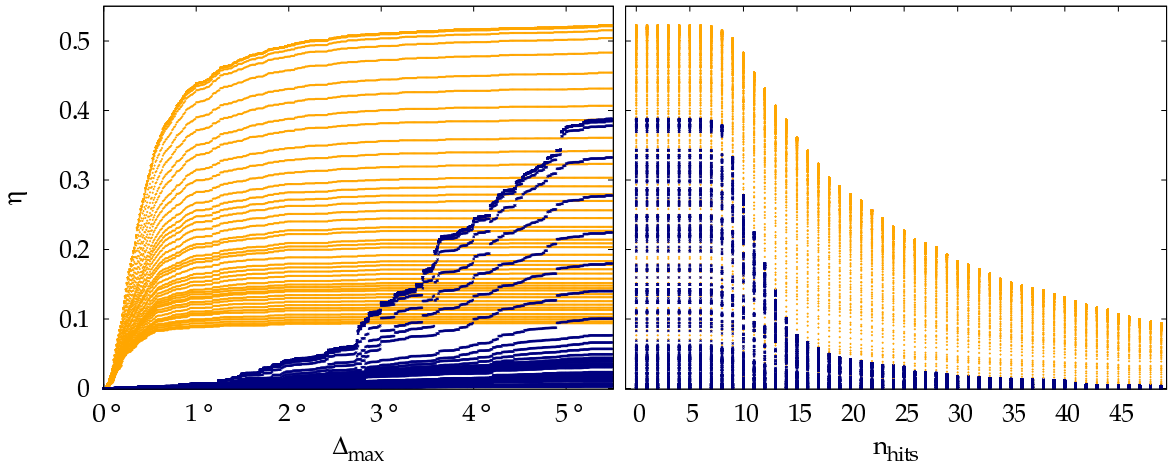

Figure 3.8.: The efficiencies η to cut on signal (orange) and background events (blue) versus the opening angle on the left–hand and the minimum number of triggered hits on the right–hand panel.The quality parameter is cut at $\Lambda = -5.3$.

be suppressed by a factor of ~ 6 when cutting on $n_{\text{hits}} \geq 15$. The statistical power also decreases for hit–cuts above 10. Consequently, a cut on n_{hits} would also significantly reduce the chance of finding a signal event. But compared to the α–dependency, $(1-\beta)$ decreases much more slowly. The proposed cut at ≥ 15, e.g., would decrease the statistical power only by a factor of $\sim$0.7. So if one would accept the loss of a few signal events, a cut on the hits at $n_{\text{hits}} = 15$ would significantly enhance the ratio of signal to expected background. Nevertheless, a cut like this should be treated with caution, as the α distribution is very steeply falling around this value (see the lower left panel of fig. 3.7). Hence, if the actual background energy distribution would be slightly different, α and thus the significance of a detection could change significantly.

EFFICIENCIES η A look at the efficiencies (see eq. 3.6) to cut signal and background events, plotted in fig. 3.8, reveals very similar dependencies to that of α and $(1-\beta)$. This is due to the fact that the efficiencies are proportional to the expected event rates μ_{b} and μ_{s}, whereas they are exponentially related to the probabilities (see eq. 3.14 and 3.15). Consequently, an optimization of the cut efficiencies would result in very similar choices for the cut parameters. If, for instance, cutting at $\Delta_{\text{max}} = 2.5°$, 50% of the signal and only $\sim$5% of the background would remain. Note that a pure cut on the reconstruction quality at $\Lambda = -5.3$ already cuts half of the signal events ($\eta = 0.5$).

3.5. LIMITS OF THE ANALYSIS

Unfortunately, not all steps in the analysis could be performed in all the desired accuracy and detail. Nevertheless, it was performed as realistic and accurate as possible. Yet still, there is room left for improvement within a more detailed investigation. A big problem for the ANTARES detector is the background, coming from atmospheric neutrinos and atmospheric muons. In this analysis, no atmospheric muon flux was included. But instead, the reported quality cut $\Lambda > -5.3$ was chosen, which should efficiently reduce this background

component (Heijboer, 2004). This work was performed in order to imitate the Gamma Ray Burst conditions as realistic as possible. But to yield high statistics without having to simulate a new large set of Monte Carlo data, previously simulated files were being used. The Gamma Ray Burst signal was not simulated separately, but imitated by adjusting the event weights. Consequently, this introduces some inaccuracies in the strategy:

The selected Monte Carlo events are equally spread on a circle of 5° around the actual GRB direction. For the background, that would be the expected distribution. But the neutrino signal of an actual burst would be expected to come from the exact burst position. In order to roughly estimate the behaviour of the data set when cutting on the angle around the GRB direction, the MC data have been treated as if they originated from the burst direction. This is of course not true. But we assume that the differences between the original and reconstructed tracks are on average similar for events coming from similar directions. Since the distance between the MC event and the GRB direction is by definition of the search cone always $\leq 5^\circ$, this assumption seems to be justified.

4. Systematic Angle Error Studies

The actual track of a muon is reconstructed from the time and position information of detected Čerenkov photons, which are emitted due to the relativistic motion of the particle through the water. Hence the precision to which the track position and direction can be reconstructed strongly depends on the photon statistics, which might introduce errors in the reconstructed Zenith and Azimuth angle. The statistical uncertainties cannot be avoided and represent the angular resolution of a certain reconstruction strategy (like, e.g., the Aart Strategy, sec. 3.2.4). Furthermore, a certain spread is introduced by the scattering of the muon with respect to the primary neutrinos direction (see section 1.2). But apart from these statistical fluctuations, it was proposed by Anton (2010) that also systematic errors could contribute. They are supposed to arise for instance from the actual position of the muon track in the detector and its orientation relative to the photo sensors, introducing a systematic tilt of the reconstructed track relative to the true muon track.

In contrast to the statistical errors, the systematic errors could, in principle, be corrected event by event. To test for the existence of such systematic shifts, Monte Carlo simulations can be used, as the 'true' Azimuth and Zenith angles of an event are still known and can be compared to the reconstructed direction. For a large number of simulations of a single event, the reconstructed angles are supposed to show a Gaussian–like distribution. The width of the Gaussian represents the statistical errors. If this distribution was furthermore shifted with respect to the original Monte Carlo angles, a systematic error could be reported. If the shift of the Gaussian distribution was larger than its width, the systematic shift could be called significant.

If for a specific muon event (defined by its energy and the position and direction of its track) a significant systematic error in the angular reconstruction is known, one could in principle correct for this. Since this requires to simulate each event a few hundred times to gain sufficient statistics, this is only realizable in analyses with few events (like, e.g., a GRB or point-source analysis). Every neutrino event detected by Antares with a reconstructed track and energy would have to be simulated a few hundred times with the very same track and energy. If then, in the Monte Carlo reconstructed angles, a shift would be reported, one would correct for it in the real data[1].

To study the feasibility of such corrections, the distribution of angular differences between the reconstructed and the true tracks for a given muon event in the detector is investigated. The width of the distribution represents the Azimuth or Zenith angular resolution which should be in the order of the overall angular resolution. The mean value $\langle \Delta\Phi \rangle$ and the sample standard deviation σ of the distribution are

[1] Note, however, that as there is no accurate energy reconstruction available, this can only be done if the systematic shifts have been shown to be independent of energy. Hence the simulations have to be performed for different energies.

$$\langle \Delta\Phi \rangle = \frac{1}{N} \sum_i^N \Delta\Phi_i = \frac{1}{N} \sum_i^N \left(\Phi_i^{Reco} - \Phi^{MC} \right) \tag{4.1}$$

$$\sigma = \sqrt{\frac{1}{N-1} \sum_i^N \left(\Phi_i - \langle \Phi \rangle \right)^2} \tag{4.2}$$

Where σ is a measure for the width of the distribution around its mean value, also called *root mean square deviation* RMSD. One can speak of a significant systematic error in the reconstructed angles as soon as the mean deviation $\langle \Delta\Phi \rangle$ from the Monte Carlo value Φ^{MC} is in the order of the standard deviation of the distribution, i.e. $\langle \Delta\Phi \rangle \gtrsim \sigma$.

A muon track with fixed energy E, velocity vector $\mathbf{v}$ and position $\mathbf{r}$ in the detector was simulated by Thomas Eberl using the ANTARES Monte Carlo detector simulation KM3 (see Navas & Thompson, 1999; Bailey, 2002b, for a description.). This program allows to fully simulate the response of the ANTARES detector to the passage of high energy muons. The first Monte Carlo generation was performed with 200 simulations for each event, the second one with 1000 to improve statistics. This was done for some events exemplary in order to study the general feasibility of such systematic error corrections.

For a preferably realistic analysis, real optical background was added in the same manner as in the GRB analysis (see section 3.2.3). The minimum bias data of run 32165 with a mean rate of 62.39 kHz was chosen, which has already been used before. For every frame in the Monte Carlo files, one minimum bias event was selected randomly and the hits were added to the MC frame. The data were then calibrated and triggered according to the respective run setup (see, again, section 3.2.3). Afterwards, the AART STRATEGY was applied to reconstruct events. The quality parameter was cut at $\Lambda \geq -5.3$ (see section 3.2.4). No further cut on the number of triggered hits was performed as this number strongly depends on the energy of the event, and is more or less in the same order for all events with the same track and energy. Subsequently, the reconstructed angle distribution is being investigated. In the following, I will first describe the effects of different chosen energies, before taking a look at the different tracks.

4.1. ENERGIES

Muon tracks with energies in the range of $E \sim 10^2\,\text{GeV} \ldots 10^8\,\text{GeV}$ have been simulated, whereas E denotes the energy of the muon when entering the can (see section 1.3.4). This is where the KM3 simulation starts.

Tracks with $\sim 10^2\,\text{GeV}$ were found to be not energetic enough to produce significant light in the detector as they lose too much energy when travelling from the can intersection point to the detector. Hence, they cannot emit sufficient Čerenkov light to be detected. The number of Monte Carlo hits after the KM3 simulation was ~ 5. In the sample of 1000 simulated events, no single frame was triggered. On the other hand, the very high energy tracks with $\sim 10^8\,\text{GeV}$ produce electromagnetic showers that induce up to ~ 900 triggered hits and more, i.e., all optical modules are detecting one or more photons. With a frame like that, no reasonable track can be reconstructed.

4.2. DIFFERENT TRACKS

Different tracks within and outside the detector have been analysed. Various effects arose, which would make a dedicated analysis to this event-by-event study worthwhile.

A) TRACK LYING OUTSIDE THE DETECTOR The first guess was that tracks lying slightly outside of the detector would show the biggest effect of systematic shifts of the reconstructed Azimuth angles with respect to the primary Monte Carlo track. A track lying $\sim 10\,\text{m}$ outside of the ANTARES detector, closest to line 1, was chosen. The muon propagates directly from West to East ($\Phi = 180^\circ$). Figures 4.1 and 4.2 show the Azimuth distributions for two events with the same track and energies of $0.87 \cdot 10^4\,\text{GeV}$ and $0.87 \cdot 10^6\,\text{GeV}$, respectively. In both cases, no obvious shift in the reconstructed Azimuth distributions can be reported. It is striking that for the $0.87 \cdot 10^4\,\text{GeV}$ track a lot of events seem to 'cluster' around preferred Azimuth values far apart from the actual value. The points around $\Phi \sim 230^\circ$, for example, show quite good reconstruction quality parameters Λ. Even with a harder cut at $\Lambda \geq -4.8$, some of the outliers would still remain. Note, nevertheless, that an additional cut on the number of hits would not improve the situation since all of the events – including the outlying points – triggered around $10 \cdots 30$ hits in the detector. These events seem to represent 'mirror solutions', resulting from the actual position of the track relative to the detector lines. They occur most probably when the reconstruction software could fit another track, mirrored for instance on one of the detector lines. It would be an interesting task to examine these effects in more detail, for instance by slightly shifting the track with respect to the line to see, when these mirror solutions appear. For the more energetic event with $0.87 \cdot 10^6\,\text{GeV}$ (fig. 4.2), these effects could not be observed. But instead, a relatively wide spread in the reconstructed Azimuth angles can be seen. The width of the distribution $\sigma \sim 0.65^\circ$ is large compared to the total angular resolution[2] of 0.34°. That means, the Azimuth resolution is much worse than the combined angular resolution of Azimuth and Zenith.

B) TRACK STRAIGHT THROUGH THE CENTRE OF ANTARES For comparison, I shifted the first track such that it would pass directly through the centre of ANTARES. The Azimuth angles (fig. 4.3) are well distributed around the original Monte Carlo angle with a spread of $\sigma \sim 0.3^\circ$ for both energies, $0.87 \cdot 10^4\,\text{GeV}$ and $0.87 \cdot 10^6\,\text{GeV}$. There might be a very slight shift to smaller angles, but the mean $\langle \Delta\Phi \rangle = -0.13^\circ$ (for the $0.87 \cdot 10^4\,\text{GeV}$ case) is smaller than the variation of the values, hence no significant shift can be reported.

C) TRACK THROUGH DETECTOR I analysed another track lying within the detector, hitting the $z = 0$ plane at $(62.58\ 84.107\ 0)\,\text{m}$ with an energy of $0.87 \cdot 10^5\,\text{GeV}$. This track is very interesting since it shows a systematic shift of the reconstructed Azimuth angles as well as the mirror solutions which also appeared in track A) (fig. 4.1). Figure 4.4 shows the reconstructed angle distribution. Again, outlying points at an Azimuth of $\sim 190^\circ$ can be observed, showing quite good Λ-values and more than 35 triggered hits. However, in this case, a harder cut, for example at $\Lambda \geq -4.8$, would exclude these points. With this

[2]The angular resolution is defined as the mean value of the angles between the reconstructed and Monte Carlo track.

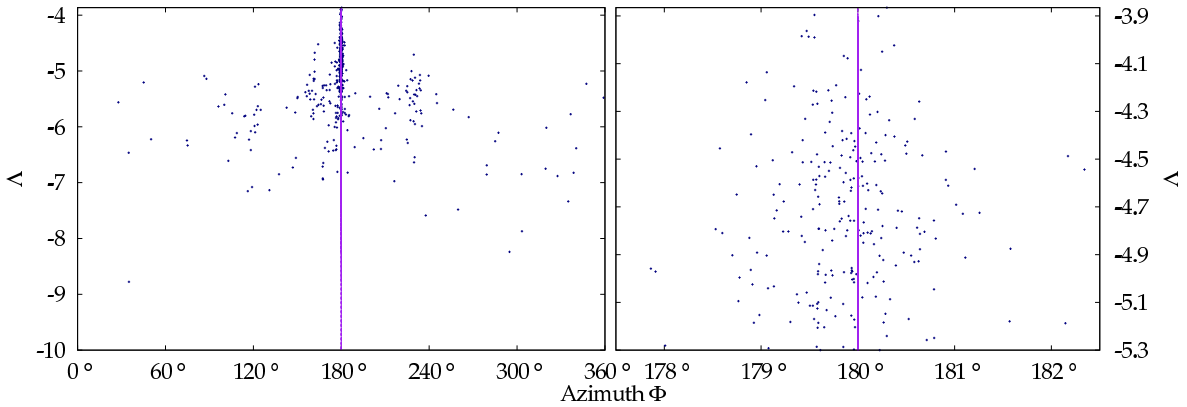

Figure 4.1.: Reconstructed Azimuth angles for a track lying $\sim 10\,\mathrm{m}$ *outside the detector with an energy of* $0.87 \cdot 10^4\,\mathrm{GeV}$ *versus the Aart reconstruction quality parameter* Λ*. The real Monte Carlo Azimuth is drawn in violet.*

harder quality cut, a systematic Azimuth shift $\langle \Delta\Phi \rangle = 0.59^\circ$ with a width of $\sigma = 0.56^\circ$ can be reported. The total angular resolution of the reconstruction is 0.39°. This event also showed a shift in the reconstructed Zenith distribution. At a quality cut of $\Lambda \geq -4.8$, the Zenith is shifted by $\langle \Delta\Theta \rangle = -0.19^\circ$ with a width of $\sigma = 0.19^\circ$. For an event like this, the angular resolution could be significantly improved by correcting for these systematic angular shifts. Note, however, that at such energies the angular uncertainties from the scattering angle Θ_S between muon and primary neutrino are well below 0.1° (see fig. 1.4).

4.3. RESULTS AND CONCLUSION

Having done these first feasibility tests, I conclude that it is most worthwhile to look for such statistical errors and mirror solutions in a dedicated analysis. It would be very interesting to see how these effects evolve when applying different reconstruction strategies like the newly available AAFIT. Further studies should include a more sophisticated analysis of the cut parameter Λ, since I could show that often enough, a pure cut on $\Lambda \geq -5.3$ is insufficient to get rid of mirror solutions. In such an analysis, it would be of great importance to study the energy dependence of the systematic angle shifts. As long as no accurate energy reconstruction is available, the correction of systematic angular errors would be only possible if the effect is known to be independent of the energy — or at least within a certain energy range, to within the event energy can be confined. In few-event studies like GRB analyses, a known systematic error in the angular reconstruction could be corrected, thereby improving the directional reconstruction of the neutrino signal.

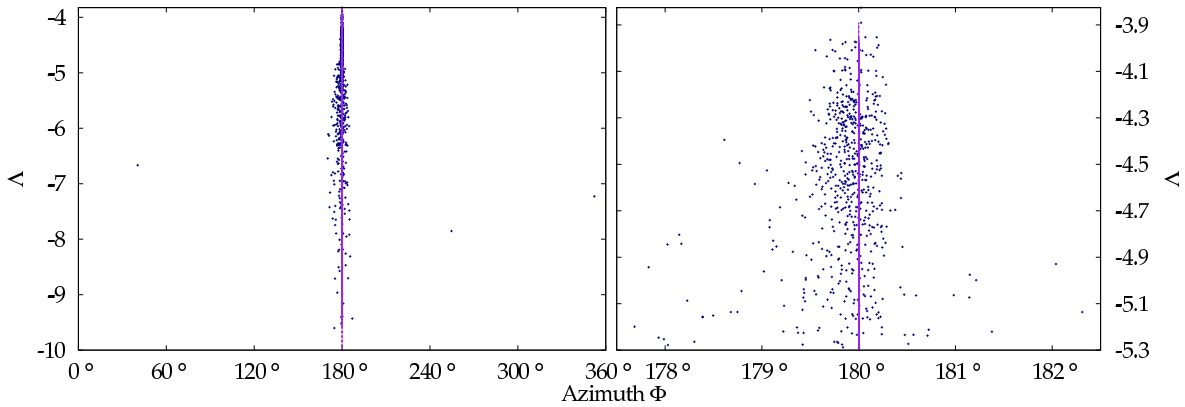

Figure 4.2.: Reconstructed Azimuth angles for a track lying $\sim 10\,\mathrm{m}$ *outside the detector with an energy of* $0.87 \cdot 10^6\,\mathrm{GeV}$*. The track is equal to the one shown in fig. 4.1, but with an energy 100 times higher.*

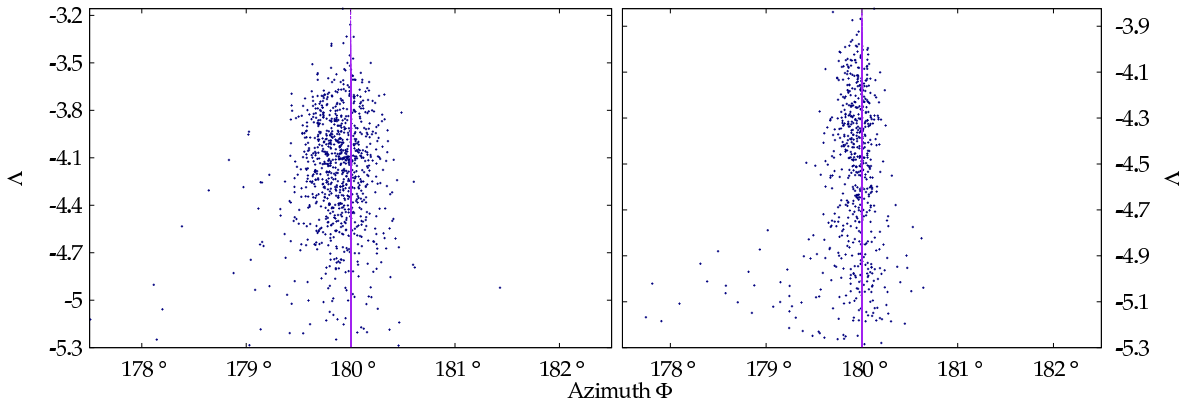

Figure 4.3.: Reconstructed Azimuth angles for a track directly through the centre of the detector with an energy of $0.87 \cdot 10^4\,\mathrm{GeV}$ *on the left hand side and* $0.87 \cdot 10^6\,\mathrm{GeV}$ *on the right hand side. No significant shift in the reconstructed Azimuth distributions could be observed.*

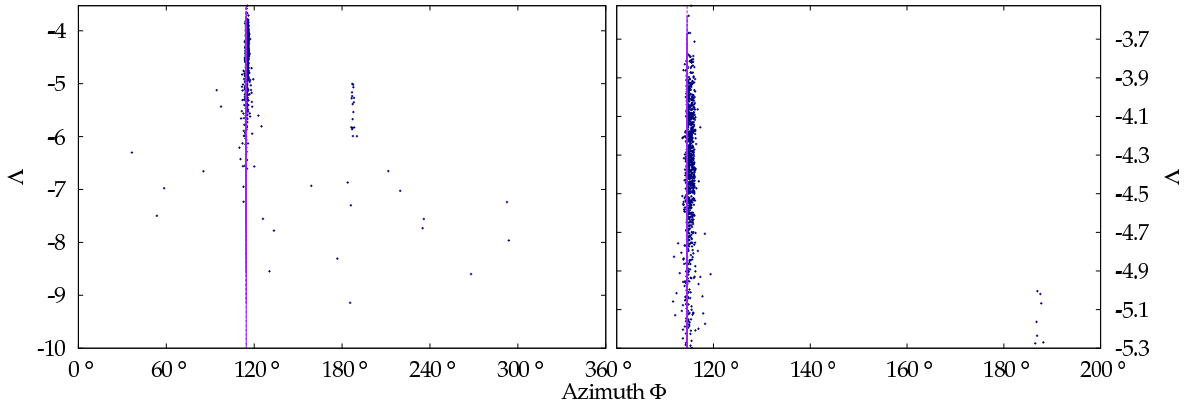

Figure 4.4.: Azimuth angle distribution for another track lying in the detector, $E = 0.87 \cdot 10^5\,\mathrm{GeV}$*. Note the mirror solutions with quite good quality parameters* Λ*.*

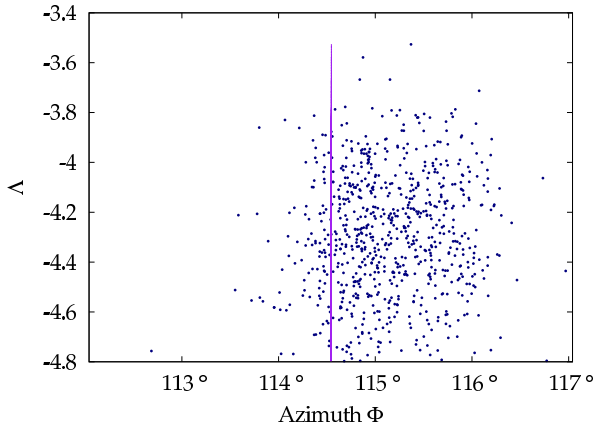

Figure 4.5: With a cut at $\Lambda \geq -4.8$, the outlying points are excluded and a systematic Azimuth shift of $+0.59°$ can be observed.

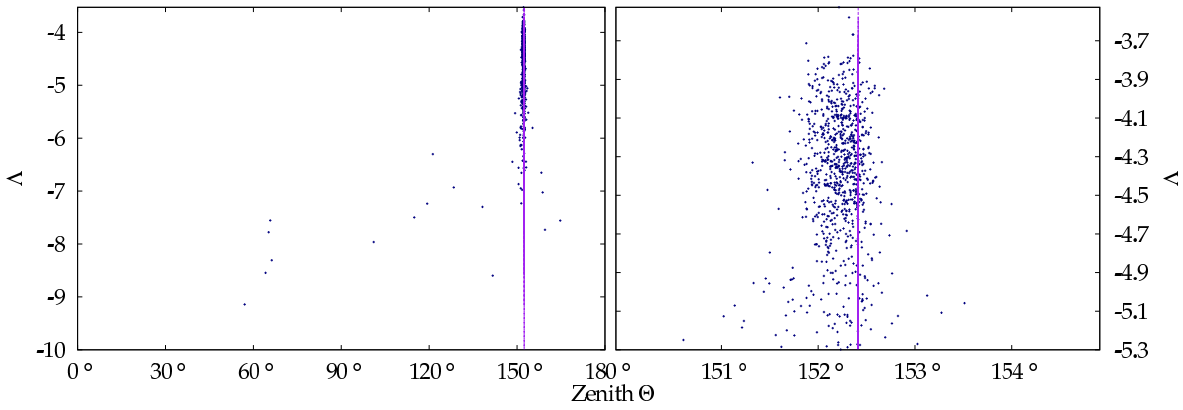

Figure 4.6.: The Zenith angle distribution for track C), $E = 0.87 \cdot 10^5\,\mathrm{GeV}$. Also a systematic shift of the reconstructed Zenith angles can be observed. A cut at $\Lambda \geq -4.8$ yields a Zenith shift of $\langle \Delta\Theta \rangle = -0.19°$ with a spread of $\sigma = 0.19°$.

5. Conclusions

5.1. GRB Analysis

In this work, I investigated a possible Gamma Ray Burst analysis with the neutrino telescope Antares. High energy neutrinos are expected to be emitted together with the observed prompt GRB photons, if protons were accelerated in the same way as electrons in the relativistic outflows during the burst. The first detection of GRB neutrinos would prove the well–established assumption of hadronic acceleration in astrophysical sources. It can also test different models and even probe general relativity. Furthermore, accelerated protons from Gamma Ray Bursts may serve to explain the Cosmic Ray flux at ultra–high energies.

Using a large set of Monte Carlo simulated data, I simulated a GRB neutrino signal and the detector response of the respective burst time as realistic as possible. For example, the actual calibration of the detector was applied to the data set and real optical background of the respective Antares data–taking run has been added to the simulated events. After reconstruction with the Aart Strategy, I optimized the analysis procedure: By cutting out events which did not fulfil certain selection criteria, the ratio of signal and background events as well as the probabilities to detect background and signal events could be influenced and improved. The analysis was performed exemplarily for the burst GRB080218B, which should have produced one of the strongest neutrino fluxes in the Antares detector, but can as well be applied to any other.

I could show that the established method of minimizing the *Model Discovery Potential* would not yield the best results in cases with very low expected background rates. The flux from atmospheric neutrinos is already so faint that a detected neutrino would always have a significance of better than 5 σ. As the MDP method tries to optimize the cuts in order to achieve a significance level of *exactly* 5 σ, it would always prefer a set of looser cuts.

It was shown that with appropriate choices for the cut parameters, the significance of a possible neutrino signal can be improved. The most promising parameter in this context is the opening angle Δ_{max}, to which a possible search for signal neutrinos can be confined. A cut at $\Delta_{\mathrm{max}} \sim 2.5^\circ$ would reduce the background–only hypothesis (α) by more than a factor of 6 with respect to a 5° search cone. The efficiency to cut on atmospheric background events would improve by a factor of ~ 4. At the same time, the probability to find the signal is still virtually at its maximum value of $(1-\beta) \sim 0.2\%$. A cut on the quality parameter tighter than at $\Lambda \geq -5.3$ does not improve the ratio of background and signal rates significantly, as their dependencies on Λ are very similar. The number of hits an event triggered in the optical modules roughly estimates the particle's energy. Consequently, this parameter can also be used to efficiently reduce the low energy background. The background–only probability falls rapidly around $n_{\mathrm{max}} \sim 10 \ldots 15$ hits, but a cut at this value would also slightly reduce the probability to detect signal events. Requiring, e.g.,

15 triggered hits would reduce the significance level α by a factor of $1/6$ while reducing $(1-\beta)$ only by 0.7.

The expected neutrino flux from Gamma Ray Bursts on Earth is not very high. Even the strongest bursts are expected to produce only around 10^{-8} neutrinos per cm^2. Yet still, it was shown that the chance to see one of these events with the ANTARES detector is around 0.2%. Hence, for samples of a few hundred bursts, the chance to see at least one neutrino is rather good. The most important result of this study is that due to the very efficiently suppressed background (the probability to detect a background neutrino is smaller than 10^{-7}), every neutrino event detected in coincidence with a GRB would most probably be produced by the burst.

5.2. SYSTEMATIC ERROR CORRECTION

I also investigated a possible method to improve analyses with only very few expected events — like the Gamma Ray Burst analysis. In ANTARES, the tracks of neutrino events (or, more precisely, the produced muon) are reconstructed by the arrival times and amplitudes of light pulses in a three–dimensional array of optical modules. The precision of the reconstruction algorithms strongly depend on the photon statistics. I investigated if — apart from the ever–present statistical uncertainties — also systematic errors in the reconstruction of the track directions are present. If such systematic shifts for a certain track are known, these can in principle be corrected for every detected event, thereby improving the angular resolution of the analysis. For a first feasibility test, I randomly chose some tracks, which were then simulated up to 1000 times in the detector in order yield high statistics. In fact, for some of these tracks I could observe systematic deviations of the reconstructed Azimuth and Zenith with respect to the original Monte Carlo angles. Consequently, I would suggest to investigate this subject further, e.g., by shifting the tracks slightly towards detector lines and especially study their energy dependence. As the energy reconstruction is still very challenging in ANTARES, the correction of angular shifts can only be performed if the systematic shifts of a certain track are known to be virtually independent of the particle's energy. Nevertheless, in principle the feasibility of systematic angular error corrections could be shown.

List of Figures

Acknowledgements

This thesis would not have been possible without the help and support of many people, to whom I owe my deepest thanks.

First of all, I would like to show my gratitude to Prof. Dr. Gisela Anton for her excellent supervision during my last research project and this thesis, including providing me with two different thesis topics.

Furthermore, I want to thank the Elite Netzwerk Bayern, who gave me the opportunity to study in the elite graduate program at the University of Erlangen–Nuremberg and Regensburg. I could benefit a lot from the intensive and individual support and especially the research projects during my studies, that gave insight into the manifold fields of modern physics. At this point, I also want to thank the respective supervisors of the projects as well as the spokesman of the elite graduate program at Erlangen, Prof. Dr. Klaus Mecke.

I am grateful for a great time I could spent at The Erlangen Centre for Astroparticle Physics (ECAP). I like to thank my colleagues at the office for a nice working atmosphere and some pleasant hours. In particular, I would like to stress out Holger Motz, whom I owe thanks for his supervision and a lot of help with the SeaTray software.

I am indebted to all the people who thoroughly read my thesis. Thanks to Holger Motz and my parents for partly reading the thesis and giving helpful comments and remarks. My special thanks goes to Thomas Dauser for patiently reading the whole thesis.

Last but not least, I owe my deepest thanks to my parents for their encouragement and uncompromising support throughout my studies and during this thesis.

REFERENCES

Abbasi R., Abdou Y., Abu-Zayyad T., et al., 2010, ApJ 710, 346

ANTARES Collaboration 2000, Astroparticle Physics 13, 127

ANTARES Collaboration 2005, Astroparticle Physics 23, 131

Anton G., 2010, Private Communication, on the Correction of Systematic Angle Errors

Bailey D., 2002a, Genhen v5r1: Software Documentation, ANTARES-Software/2002-004

Bailey D., 2002b, KM3 v2r1: User Guide, ANTARES-Software/2002-006

Barr G.D., Gaisser T.K., Lipari P., et al., 2004, Phys. Rev. D 70, 023006

Becker J.K., 2008 458, 173

Bouwhuis M., 2005, Ph.D. thesis, Universiteit van Amsterdam

Brunner J., 1999, Updated tag list for the new ANTARES event format, ANTARES-Software/1999-003

Dermer C.D., Razzaque S., 2010, ApJ 724, 1366

Eberl T., Kopper C., 2009, The SeaTray software framework, ANTARES-Software/2009-013

Eichler D., Livio M., Piran T., Schramm D.N., 1989, Nat 340, 126

Fiore F., Guetta D., Piranomonte S., et al., 2006, Nuovo Cimento B Serie 121, 1395

Galama T.J., Vreeswijk P.M., van Paradijs J., et al., 1998, Nat 395, 670

Goodman J., 1986, Astrophys. J., Lett. 308, L47

Guetta D., Hooper D., Alvarez-Muñiz J., et al., 2004, Astroparticle Physics 20, 429

Heijboer A.J., 2004, Ph.D. thesis, Universiteit van Amsterdam

Hill G.C., Hodges J., Hughey B., et al., 2006, In: L. Lyons & M. Karagöz Ünel (ed.) Statistical Problems in Particle Physics, Astrophysics and Cosmology., p.108

Kappes A., Katz U., 2005, On the Use of Event Weights for the Simulation of Atmospheric Muons in ANTARES, ANTARES-Software/2005-003

Klebesadel R.W., Strong I.B., Olson R.A., 1973, ApJ 182, L85+

Kouveliotou C., Meegan C.A., Fishman G.J., et al., 1993, Astrophys. J., Lett. 413, L101

Longair M.S., 1994, High energy astrophysics. Volume 2. Stars, the Galaxy and the interstellar medium.

Meegan C.A., Fishman G.J., Wilson R.B., et al., 1992, Nat 355, 143

Mészáros P., 2006, Reports on Progress in Physics 69, 2259

Metzger M.R., Djorgovski S.G., Kulkarni S.R., et al., 1997, Nat 387, 878

Navas S., Thompson L., 1999, KM3 User Guide and Reference Manual, ANTARES-Software/1999-011

Paciesas W.S., Meegan C.A., Pendleton G.N., et al., 1999, ApJS 122, 465

Particle Data Group 2008, Physics Letters B 667

Piran T., 1998, In: H. Sato & N. Sugiyama (ed.) Frontiers Science Series 23: Black Holes and High Energy Astrophysics., p.217

Preece R.D., Briggs M.S., Giblin T.W., et al., 2002, ApJ 581, 1248

Razzaque S., Mészáros P., Waxman E., 2003, Phys. Rev. D 68, 083001

Rees M.J., Meszaros P., 1992, MNRAS 258, 41P

Rhoads J.E., 1997, Astrophys. J., Lett. 487, L1+

Sari R., Piran T., 1997, ApJ 485, 270

Sari R., Piran T., Narayan R., 1998, Astrophys. J., Lett. 497, L17+

Schady P., 2008, GRB Coordinates Network 7323, 1

Schady P., Evans P.A., Krimm H., 2008, GCN Report 117, 1

Shemi A., Piran T., 1990, Astrophys. J., Lett. 365, L55

Sinervo P.K., 2002, ArXiv High Energy Physics - Experiment e-prints

UK Swift Science Data Centre 2010, Gamma–Ray Bursts Coordinates Network, CTAN: `http://www.swift.ac.uk/gcn.shtml`

Waxman E., 1995a, Physical Review Letters 75, 386

Waxman E., 1995b, Astrophys. J., Lett. 452, L1+

Waxman E., 2000, ApJS 127, 519

Waxman E., Bahcall J., 1997, Physical Review Letters 78, 2292

Waxman E., Bahcall J.N., 2000, ApJ 541, 707

Woosley S.E., Bloom J.S., 2006, ARA&A 44, 507

A. Probabilities α and $(1-\beta)$

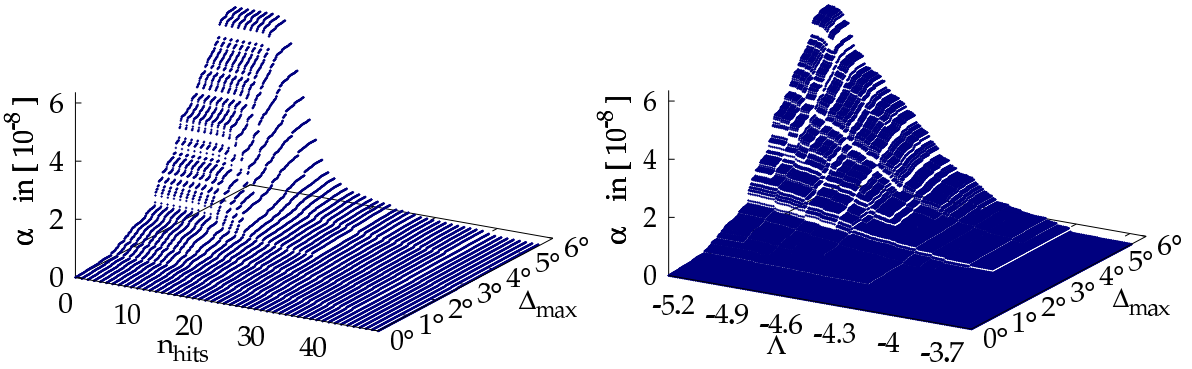

Figure A.1.: The probability α versus the different cutting parameters opening angle, number of triggered hits and the quality parameter Λ. For the left–hand panel, the cut on the reconstruction quality was fixed to $\Lambda > -5.3$ whereas for the right–hand one, the number of triggered hits was not cut on, i.e., $n_{hits} = 0$.

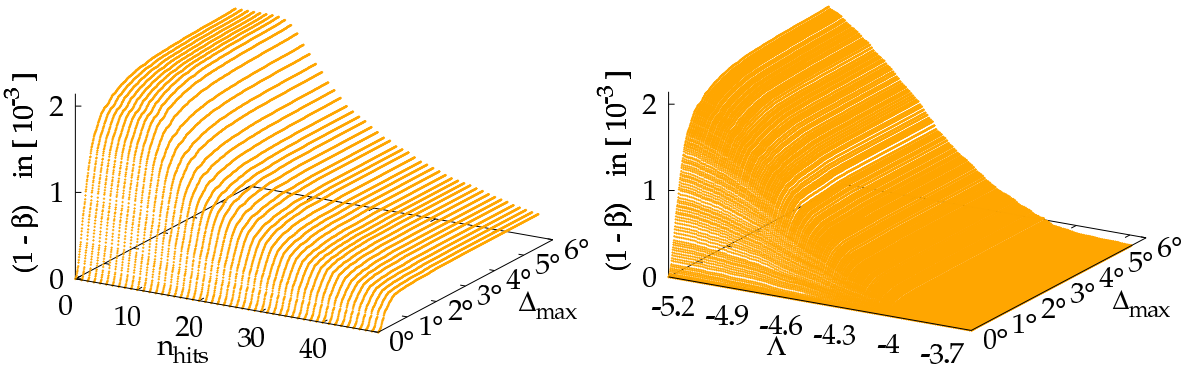

Figure A.2.: The dependency of $(1-\beta)$ on the cut parameters. For each of these plots, the third cut parameter was fixed as described in fig. A.1.

ERKLÄRUNG

Hiermit erkläre ich, dass ich die Arbeit selbstständig angefertigt und keine anderen als die angegebenen Hilfsmittel verwendet habe.

Erlangen, den 26.01.2011

Julia Schmid